Adaptive reduced basis finite element heterogeneous multiscale method

Assyr Abdulle, Yun Bai

ANMC, Section de Mathématiques, École Polytechnique Fédérale de Lausanne, 1015 Lausanne, Switzerland,{assyr.abdulle,yun.bai}@epfl.ch

Abstract

An adaptive reduced basis finite element heterogeneous multiscale method (RB-FE-HMM) is proposed for elliptic problems with multiple scales. The multiscale method is based on the RB-FE-HMM introduced in [A. Abdulle and Y. Bai, J. Comput. Phys, 2012, in press]. It couples a macroscopic solver with effective data recovered from the solution of micro problems solved on sampling domains. Unlike classical numerical homogenization methods, the micro problems are computed in a finite dimensional space spanned by a small number of accurately computed representative micro solutions (the reduced basis) obtained by a greedy algorithm in an offline stage. In this paper we present a residual-based a posteriori error analysis in the energy norm as well as an a posteriori error analysis in quantities of interest. For both type of adaptive strategies, rigorous a posteriori error estimates are derived and corresponding error estimators are proposed. In contrast to the adaptive finite element heterogeneous multiscale method (FE-HMM), there is no need to adapt the micro mesh simultaneously to the macroscopic mesh refinement. Up to an offline preliminary stage, the RB-FE-HMM has the same computational complexity as a standard adaptive FEM for the effective problem. Two and three dimensional numerical experiments confirm the efficiency of the RB-FE-HMM and illustrate the improvements compared to the adaptive FE-HMM.

Keywords: numerical homogenization, reduced basis method, residual based adaptive FEM, quantity of interest, heterogeneous multiscale method

1. Introduction

A basic problem for many applications is the characterization of effective properties of a physical process occurring on multiple scales (e.g., elastic properties of composite materials, fluid flow through heterogeneous porous media, thermal diffusion in composite structures, etc). Such problems are often modeled by partial differential equations (PDEs) with highly oscillating coefficients varying over multiples scales, whose numerical solution is difficult to compute (if not impossible) with classical numerical methods such as the finite element method (FEM). Indeed, the computational cost needed to resolve the smallest scale in the problem is often overwhelming. Simply ignoring the fine scales does usually not allow to capture the correct effective behavior. The development of multiscale methods capable of

capturing the effective behavior of a problem without scale resolution on the whole computational domain has therefore received major attention during the past few years [1, 2, 3, 4, 5].

In this paper we focus on the finite element heterogeneous multiscale method (FE-HMM), a numerical homogenization method developed in the framework of the heterogeneous multiscale method (HMM) proposed in [6]. The main idea of the FE-HMM is to apply a macro FEM based on a macro partition of the computational domain with effective coefficients recovered (on the fly) by solving micro finite element (FE) problems defined on sampling domains located at quadrature points within each element of the macro partition (see [7] for a review). The fully discrete error analysis in [8] indicates that the optimal convergence rates can be obtained only when the macro and micro meshes are refined simultaneously. This simultaneous mesh refinement leads to superlinear growth (in the macro degrees of freedom) of the computational work. This becomes an issue (as for most of the numerical homogenization methods) for high dimensional problems or high order macro FEMs.

To address the computational issue of simultaneous macro and micro mesh refinement the reduced basis finite element heterogeneous multiscale method (RB-FE-HMM) has been introduced in [9]. Departing from the approach used in the FE-HMM, the RB-FE-HMM allows one to design an efficient numerical method relying only on a small number of micro problems selected by a rigorous a posteriori error estimator computed accurately in an so-called offline stage. In a so-called online stage, the effective solution is obtained from the macro solver of the FE-HMM with effective coefficients recovered from micro problems solved in the precomputed RB space. This method, that follows the offline-online strategy of reduced basis (RB) method [10, 11, 12, 13, 14], does no longer require the simultaneous refinement of macro and micro meshes. As illustrated in [9], the RB-FE-HMM is specially attractive for high order macro methods or three dimensional multiscale computations.

In this paper we discuss a posteriori error control and mesh refinement strategy for the RB-FE-HMM. In practice, being able to refine the computational mesh adaptively, based on a given actual numerical solution is of prime importance. Adaptive methods not only provide a criterion that indicates whether a certain prescribed accuracy is met, but also estimate local errors that allow to drive a mesh refinement that equi-distributes the approximation error (e.g., refining in the region where singularity in the solution or in the domain occur). The general adaptive strategy for the adaptive FEM is based on the following cycle

$$\text{Solve} \rightarrow \text{Estimate} \rightarrow \text{Mark} \rightarrow \text{Refine}.$$

The procedure can be understood as follows. One first solves the partial differential equation numerically on the current mesh and compute an a posteriori error by defining suitable error estimators that give an estimation of the actual error between the computed and the true solution (in a certain norm). Then, according to the distribution of the error estimator in each element, one marks the elements which have the largest contribution to the estimated error, refines the marked elements and goes back to the step 'Solve'. The essential step for adaptive method is the construction of reliable error estimator. While there is a large literature for single scale adaptive methods (see for example [15, 16, 17, 18] and the references therein), adaptive multiscale methods are still at an early stage of development. One difficulty is that

the error estimator (that first need to be suitably modeled) depends on multiple scales and the reliability of such error estimator depends on the accuracy of the resolution of the fine scale.

A posteriori error analysis for the FE-HMM has first been given in [19] based on a two-scale analysis [20]. A posteriori error analysis for the FE-HMM in the physical energy-norm has been derived in [21] and the extension of the FE-HMM to goal oriented adaptivity (in quantities of interest) has been discussed in [22]. For this latter adaptive method, the solution of dual problems (in a higher macro FE space) are required. Both adaptive methods [21, 22] have proved to be useful and more efficient than the FE-HMM with uniform refinement when the macroscopic domain or the macroscopic solution exhibit singularities. But as mentioned above, the simultaneous mesh refinement still represents a significant computational overhead that prevents to solve efficiently three-dimensional problems adaptively, or to use adaptive higher order macro FEM. In this paper we discuss a new adaptive method that combines RB techniques with the FE-HMM. This method, that allows to drive a macroscopic mesh refinement using the same precomputed set of RB micro functions to estimate the effective data, improves significantly the adaptive FE-HMM and provides a highly efficient adaptive multiscale computational strategy.

The paper is organized as follows. In Section 2, we briefly review the FE-HMM and the RB-FE-HMM. The residual based adaptive RB-FE-HMM is discussed in Section 3 and the corresponding a posteriori estimates for the upper and lower bound are derived in the energy norm. The goal-oriented adaptive RB-FE-HMM is presented in Section 4, where an exact representation of the error in a quantity of interest is derived. Numerical examples for the proposed method in two and three dimensions and comparison with the adaptive FE-HMM are presented in section 5.

Notations Let $\Omega \subset \mathbb{R}^d$ be an open set, and $Y = (-\frac{1}{2}, \frac{1}{2})^d$. Denote the standard Sobolev Space by $W^{\ell,p}(\Omega)$. For $p = 2$, we sometimes use the notation $W^{\ell,p}(\Omega) = H^\ell(\Omega)$. $H_0^1(\Omega)$ denotes the closure of $C_0^\infty(\Omega)$ in $H^1(\Omega)$. We define $H^1_{per}(Y) := \{g \in H^1(Y) |\ g \text{ periodic in } Y\}$. We also have the property that $H^1_{per}(Y) = \overline{C^\infty_{per}(Y)}$, where $C^\infty_{per}(Y)$ is a subspace of $C^\infty(\mathbb{R}^d)$ of periodic functions in the cube Y.

2. Model problem, FE-HMM and RB-FE-HMM.

In this section, we briefly discuss the type of problems that we consider and review the classical homogenization. We also recall the reduced basis heterogeneous multiscale method (RB-FE-HMM) recently introduced in [9] that we will use throughout the paper to develop an adaptive multiscale method.

Model problem. Let Ω be a bounded polyhedron in $\mathbb{R}^d$ with $d \leq 3$. We consider a second-order elliptic problems of the form

$$\begin{aligned} -\nabla \cdot (a^\varepsilon(x)\nabla u^\varepsilon(x)) &= f \quad \text{in } \Omega, \\ u^\varepsilon(x) &= 0 \quad \text{on } \partial\Omega, \end{aligned} \tag{2.1}$$

where the tensor a^ε oscillates on a small spatial scale ε and $f \in H^{-1}(\Omega)$. Here, a zero Dirichlet boundary condition is taken for simplicity. We emphasize that the numerical method presented below can be readily generalized to other boundary conditions such as non-zero Dirichlet or Neumann boundnary conditions. The $d \times d$ matrix $a^\varepsilon(x)$ is assumed to be uniformly elliptic and bounded, i.e.,

$$\lambda|\xi|^2 \leq a^\varepsilon(x)\xi \cdot \xi, \ |a^\varepsilon(x)\xi| \leq \Lambda|\xi|, \ \forall \xi \in \mathbb{R}^d, \forall \varepsilon > 0, \tag{2.2}$$

for a.e $x \in \Omega$.

Using homogenization theory, one can prove that there exists $u^0 \in H_0^1(\Omega)$ such that $u^\varepsilon \rightharpoonup u^0$ weakly in $H_0^1(\Omega)$, $a^\varepsilon \nabla u^\varepsilon \rightharpoonup a^0 \nabla u^0$ weakly in $(L^2(\Omega))^d$, where u^0 is the solution of the homogenized equation (for example, see [23, 24] for detail),

$$\begin{aligned} -\nabla \cdot (a^0 \nabla u^0(x)) &= f(x) \quad \text{in } \Omega, \\ u^0(x) &= 0 \quad \text{on } \partial\Omega, \end{aligned} \tag{2.3}$$

where a^0 is the homogenized tensor. As a^0 is usually unknown, we need to introduce numerical methods for its approximation. One well-known method is the FE-HMM which is based on a macroscopic FEM with quadrature formula (QF) defined on a macro partition of the domain Ω, supplemented by microscopic FEMs applied on sampling domains centered at the macroscopic quadrature points of the QF to estimate the unknown data in the macro system.

2.1. The FE-HMM

We first defined a macro finite element (FE) space

$$S_0^\ell(\Omega, \mathcal{T}_H) = \{v^H \in H_0^1(\Omega); \ v^H|_K \in \mathcal{R}^\ell(K), \ \forall K \in \mathcal{T}_H\},$$

where $\mathcal{T}_H$ is a family of (macro) partitions of Ω in simplicial or quadrilateral elements K of diameter H_K, and $\mathcal{R}^\ell(K)$ is the space $\mathcal{P}^\ell(K)$ of polynomials on K of total degree at most ℓ if K is a simplicial FE, or the space $\mathcal{Q}^\ell(K)$ of polynomials on K of degree at most ℓ in each variable if K is a quadrilateral FE. For a given macro partition, we define as usual $H := \max_{K \in \mathcal{T}_H} H_K$. We note that H in our discretization is allowed to be much larger than ε. Defining a QF $\{\hat{x}_j, \hat{\omega}_j\}_{j=1}^J$ on a reference element $\hat{K}$, we equip each element K with a corresponding QF $\{x_{K_j}, \omega_{K_j}\}_{j=1}^J$ by using a C^1-diffeomorphism. We assume positive weights $\hat{\omega}_j > 0, \ j = 1, \ldots, J$ and make the following assumptions on the quadrature formula (similar to the requirement for standard FEM with numerical quadrature [25])

(**Q1**) $\quad \sum_{j=1}^J \hat{\omega}_j |\nabla \hat{p}(\hat{x}_j)|^2 \geq \hat{\lambda} \|\nabla \hat{p}\|^2_{L^2(\hat{K})}, \ \forall \hat{p}(\hat{x}) \in \mathcal{R}^\ell(\hat{K}), \ \text{with } \hat{\lambda} > 0;$

(**Q2**) $\int_{\hat{K}} \hat{p}(\hat{x}) d\hat{x} = \sum_{j \in J} \hat{\omega}_j \hat{p}(\hat{x}_j), \ \forall \hat{p}(\hat{x}) \in \mathcal{R}^\sigma(\hat{K})$, where $\sigma = \max(2\ell - 2, \ell)$ if $\hat{K}$ is a simplicial FE, or $\sigma = \max(2\ell - 1, \ell + 1)$ if $\hat{K}$ is a rectangular FE.

For each macro element $K \in \mathcal{T}_H$ and each integration point $x_{K_j} \in K$, $j = 1, \ldots, J$, we define the sampling domains $K_{\delta_j} = x_{K_j} + (-\delta/2, \delta/2)^d$, $(\delta \geq \varepsilon)$. For a sampling domain K_{δ_j}, we

then define a micro FE space $S^q(K_{\delta_j}, \mathcal{T}_h) \subset W(K_{\delta_j})$ with simplicial or quadrilateral FEs and piecewise polynomial of degree q, where $\mathcal{T}_h$ is a conformal and shape regular family of triangulations. The space $W(K_{\delta_j})$ is either the Sobolev space

$$W(K_{\delta_j}) = W^1_{per}(K_{\delta_j}) = \{z \in H^1_{per}(K_{\delta_j});\ \int_{K_{\delta_j}} z dx = 0\} \tag{2.4}$$

for a periodic coupling or

$$W(K_{\delta_j}) = H^1_0(K_{\delta_j}) \tag{2.5}$$

for a coupling with Dirichlet boundary conditions.

At the macroscopic level, the numerical methods is defined as follows: find $u^H \in S^\ell_0(\Omega, \mathcal{T}_H)$ such that

$$B_H(u^H, v^H) = \int_\Omega f v^H dx,\ \forall v^H \in S^\ell_0(\Omega, \mathcal{T}_H), \tag{2.6}$$

where

$$B_H(v^H, w^H) := \sum_{K \in \mathcal{T}_H} \sum_{j=1}^{J} \frac{\omega_{K_j}}{|K_{\delta_j}|} \int_{K_{\delta_j}} a^\varepsilon(x) \nabla v^h_{K_j}(x) \cdot \nabla w^h_{K_j}(x) dx. \tag{2.7}$$

In (2.7) $v^h_{K_j}$ (respectively $w^h_{K_j}$) denotes the solution of the following micro problem: find $v^h_{K_j}$ such that $v^h_{K_j} - v^H_{lin,j}(x) \in S^q(K_{\delta_j}, \mathcal{T}_h)$ and

$$\int_{K_{\delta_j}} a^\varepsilon(x) \nabla v^h_{K_j}(x) \cdot \nabla z^h(x) dx = 0 \quad \forall z^h \in S^q(K_{\delta_j}, \mathcal{T}_h), \tag{2.8}$$

where we used the notation $v^H_{lin,j}(x) := v^H(x_{K_j}) + (x - x_{K_j}) \cdot \nabla v^H(x_{K_j})$.

It is proved in [7, Lemma 5][8] that $B_H(\cdot, \cdot)$ is bounded and coercive. Hence, by Lax-Milgram Theorem, there exists unique solution u^H of (2.6).

A priori estimates. The following estimates hold provided suitable regularity assumptions on $a^0(x)$ (see [7, 8, 26]):

$$\begin{aligned} \left\|u^0 - u^H\right\|_{H^1(\Omega)} &\leq C\left(H^\ell + r_{MIC} + r_{MOD}\right), \\ \left\|u^0 - u^H\right\|_{L^2(\Omega)} &\leq C\left(H^{\ell+1} + r_{MIC} + r_{MOD}\right). \end{aligned} \tag{2.9}$$

To estimate the micro error, it is convenient to make the following assumption on $\psi^i_{K_j}$, the exact solution of Problem (2.8), i.e., the solution of $\int_{K_{\delta_j}} a^\varepsilon(x) \nabla(\psi^i_{K_j}(x) + x_i) \cdot \nabla z(x) dx = 0 \quad \forall z \in W(K_{\delta_j}),\ i = 1, \ldots, d$ [27, 28]

(**H1**) Given $q \in \mathbb{N}$, the cell functions $\psi^i_{K_j}$ satisfy

$$|\psi^i_{K_j}|_{H^{q+1}(K_{\delta_j})} \leq C\varepsilon^{-q}\sqrt{|K_{\delta_j}|},$$

with C independent of $i = 1 \dots d$, ε, the quadrature point x_{K_j} and the domain K_{δ_j}.

Then, the microscopic error r_{MIC} can be bounded by [8, 27, 28]

$$r_{MIC} \leq C \left(\frac{h}{\varepsilon}\right)^{2q}. \tag{2.10}$$

Finally, assuming

$$a^\varepsilon(x) = a(x, \frac{x}{\varepsilon}) = a(x, y) \text{ Y-periodic in } y, \tag{2.11}$$

the modeling error r_{MOD} can be bounded as follows [26, 29]

$$r_{MOD} = 0 \qquad \text{if } W(K_{\delta_j}) = W^1_{per}(K_{\delta_j}) \text{ and } \delta/\varepsilon \in \mathbb{N}, \text{[1]} \tag{2.12}$$

$$r_{MOD} \leq C(\delta + \frac{\varepsilon}{\delta}) \qquad \text{if } W(K_{\delta_j}) = H^1_0(K_{\delta_j}) \ (\delta > \varepsilon). \tag{2.13}$$

Complexity of the FE-HMM. We write $\hat{h} = \frac{h}{\varepsilon}$ and denote by $M_{mic} = \mathcal{O}(\hat{h}^{-d})$ the number of degrees of freedom (DOF) for the micro FEM, and by M_{mac} the number of DOF of the macro FEM. We emphasize here that M_{mic} is actually independent of ε for sampling domain K_{δ_j} where $K_{\delta_j} = \delta^d = (\frac{\delta}{\varepsilon})^d \varepsilon^d = C\varepsilon^d$ with C a moderate constant (assuming that δ scales as $\delta = \hat{C}\epsilon$). For quasi-uniform macro meshes, the macro meshsize H and the micro meshsize $\hat{h}$ are related to M_{mac} and M_{mic} as

$$H = \mathcal{O}(M_{mac}^{-1/d}), \qquad \hat{h} = \mathcal{O}(M_{mic}^{-1/d}).$$

In view of (2.9) and (2.10), optimal macroscopic convergence rates (up to a modeling error r_{MOD} independent of H, h) are obtained for quasi-uniform microscopic meshsizes given by

$$\hat{h} \simeq H^{\frac{\ell}{2q}} \quad \text{for the } H^1 \text{ norm}, \quad \hat{h} \simeq H^{\frac{\ell+1}{2q}} \quad \text{for the } L^2 \text{ norm}.$$

The corresponding complexity in term of macro DOF reads

$$\underbrace{H^{-d}}_{M_{mac}} \cdot \underbrace{H^{\frac{-d\ell}{2q}}}_{M_{mic}} \cdot n_s = (M_{mac})^{1+\frac{\ell}{2q}} \cdot n_s \qquad \text{for the } H^1 \text{ norm},$$

$$\underbrace{H^{-d}}_{M_{mac}} \cdot \underbrace{H^{\frac{-d(\ell+1)}{2q}}}_{M_{mic}} \cdot n_s = (M_{mac})^{1+\frac{\ell+1}{2q}} \cdot n_s \qquad \text{for the } L^2 \text{ norm},$$

where n_s denotes the number of sampling domains per macro element $K \in \mathcal{T}_H$. As first noticed in [8] the overall complexity of the method is a function of M_{mac} and M_{mic} and is in general superlinear with respect to the macro DOF.

[1] For this estimate to hold, one needs to consider a suitable modification of the bilinear form (2.7) and the micro problem (2.8), namely one has to collocate the term $a(x, \frac{x}{\varepsilon})$ in the slow variable $a(x_{K_j}, \frac{x}{\varepsilon})$ in both (2.7) and (2.8).

2.2. The RB-FE-HMM

In this subsection, we will briefly recall the RB-FE-HMM introduced in [9] which is used in later sections to develop efficient adaptive multiscale methods. The RB-FE-HMM is based on an offline-online strategy. In the offline stage, the basis functions that span a low dimensional approximation space of the infinite dimensional space formed by the solutions of cell problems (parametrized with respect to the locations of the sampling domains) are constructed. Thanks to the pre-computation of the offline stage, the computation of the cell problems of the FE-HMM in the online stage can be done in a fixed dimensional space with low degrees of freedom independent of the macro mesh. We briefly recall this construction.

Parametrized micro problems. We use $S^q(K_{\delta_j},\mathcal{N})$ instead of $S^q(K_{\delta_j},\mathcal{T}_h)$ for the micro FE space to emphasize the DOF of the micro FEM denoted by $\mathcal{N}$, where $\mathcal{N}=\mathcal{O}(\hat{h}^{-d})$. Likewise, we use $v_{\mathcal{N},K_j}$ instead of $v^h_{K_j}$ to describe the solution of problem (2.8). We first notice that

$$v_{\mathcal{N},K_{\delta_j}}(x)=v^H_{lin,j}(x)+\sum_{i=1}^{d}\chi^i_{\mathcal{N},K_j}(x)\frac{\partial v^H_{lin,j}}{\partial x_i}, \tag{2.14}$$

where $\chi^i_{\mathcal{N},K_j}(x),\ i=1,\dots,d$ are solutions of

$$\int_{K_{\delta_j}} a^\varepsilon(x)\nabla\chi^i_{\mathcal{N},K_j}(x)\cdot\nabla z_{\mathcal{N}}(x)dx=-\int_{K_{\delta_j}} a^\varepsilon(x)\mathbf{e_i}\cdot\nabla z_{\mathcal{N}}(x)dx\quad\forall z_{\mathcal{N}}\in S^q(K_{\delta_j},\mathcal{N}). \tag{2.15}$$

In the above formula, the vector $\mathbf{e_i}$, $i=1\dots d$ denote the canonical basis of $\mathbb{R}^d$. We now map a sampling domain K_{δ_j} in the reference domain Y through $x=G_{x_{K_j}}(y)=x_{K_j}+\delta y$ and consider $\hat{\chi}^i_{\mathcal{N},K_j}$ the solution of

$$\begin{aligned} b(\hat{\chi}^i_{\mathcal{N},K_j},\hat{z}_{\mathcal{N}}) &:= \int_Y a_{x_{K_j}}(y)\nabla\hat{\chi}^i_{\mathcal{N},K_j}(y)\cdot\nabla\hat{z}_{\mathcal{N}}(y)dy \\ &= -\int_Y a_{x_{K_j}}(y)\mathbf{e_i}\cdot\nabla\hat{z}_{\mathcal{N}}(y)dy=:l_i(\hat{z}_{\mathcal{N}})\ \ \forall\hat{z}_{\mathcal{N}}\in S^q(Y,\mathcal{N}). \end{aligned} \tag{2.16}$$

We note that $a^\varepsilon(G_{x_{K_j}}(y))$ can be parametrized by $x_{K_j}\in\Omega$ and we therefore use the notation $a_{x_{K_j}}(y):=a^\varepsilon(G_{x_{K_j}}(y))$. The space $S^q(Y,\mathcal{N})$ is an FE space for the reference cell Y with the triangulation $\mathcal{T}_{\hat{h}}$.

Let $T_\delta=x_\tau+(-\delta/2,\delta/2)^d$ be a sampling domain centered at $x_\tau\in\Omega$, chosen such that $T_\delta\subset\Omega$ and let $\mathbf{e}_\eta$ be a vector of the canonical basis of $\mathbb{R}^d$. For $\{(T_\delta,\mathbf{e}_\eta);T_\delta\subset\Omega,\eta=1,\dots,d\}$, we define the space formed by the solutions of the cell problems parametrized with respect to the location of the sampling domains by

$$\mathcal{M}^{\mathcal{N}}(Y):=\{\hat{\xi}^\eta_{\mathcal{N},T_\delta};T_\delta\subset\Omega,\ \eta=1,\dots,d\}, \tag{2.17}$$

where $\hat{\xi}^\eta_{\mathcal{N},T_\delta}(\cdot):Y\to\mathbb{R}$ are the solutions of (2.16) associated with the mapping G_{x_τ}, i.e., with a tensor $a_{x_\tau}(y)=a^\varepsilon(G_{x_\tau}(y))$ and with right-hand side $l_\eta(\cdot)$. The reduced basis (RB)

functions $\hat{\xi}^{\eta}_{\mathcal{N},T_\delta}$ are computed very accurately. The DOF $\mathcal{N}$ of the FE space $S^q(Y,\mathcal{N})$ is thus assumed to be large.

As emphasized in the RB literature, the efficiency of the method relies on the affine representation of the data used for the RB strategy, here, the oscillating tensor,

$$a_{x_\tau}(y) = \sum_{q=1}^{Q} \Theta_q(x_\tau) a_q(y), \ \forall y \in Y. \tag{2.18}$$

However for general tensors $a^\varepsilon(x)$, the representation (2.18) is not available directly and we need to define an affine approximation of the tensor. One successful method is the so called empirical interpolation method (EIM) which is also an offline-online strategy. Details of the EIM can be found in [30, 31]. For simplicity, we assume in what follows that (2.18) is available (notice that we will use tensors that are not in the form (2.18) in our numerical examples and the EIM strategy will therefore be used).

A posteriori error estimator. We assume that $S_l(Y)$ is an l-dimensional linear subspace of $S^q(Y,\mathcal{N})$ and consider ξ^i_{l,T_δ} the solution of (2.16) in $S_l(Y)$ with right-hand side $l_i(\cdot)$. Let $\xi^i_{\mathcal{N},T_\delta} \in S^q(Y,\mathcal{N})$, and define

$$\hat{e}^i_{l,T_\delta} = \hat{\xi}^i_{l,T_\delta} - \hat{\xi}^i_{\mathcal{N},T_\delta}. \tag{2.19}$$

Using (2.16) we see that

$$b(\hat{e}^i_{l,T_\delta}, \hat{z}_\mathcal{N}) = b(\hat{\xi}^i_{l,T_\delta}, \hat{z}_\mathcal{N}) - l_i(\hat{z}_\mathcal{N}), \ \forall \hat{z}_\mathcal{N} \in S^q(Y,\mathcal{N}). \tag{2.20}$$

The right-hand side defines a linear form on $S^q(Y,\mathcal{N})$. Hence by the Riesz theorem, there exists a unique $\bar{e}^i_{l,T_\delta} \in S^q(Y,\mathcal{N})$ such that

$$b(\hat{e}^i_{l,T_\delta}, \hat{z}_\mathcal{N}) = (\bar{e}^i_{l,T_\delta}, \hat{z}_\mathcal{N})_\mathcal{W}, \tag{2.21}$$

where $(\cdot,\cdot)_\mathcal{W}$, defined as $(v,w)_\mathcal{W} = \int_Y \nabla v \cdot \nabla w dy$, denotes the scalar product in the space $W(Y)$ given in (2.4) or (2.5). In view of $\lambda \|\nabla \hat{e}^i_{l,T_\delta}\|^2_{L^2(Y)} \leq (\bar{e}^i_{l,T_\delta}, \hat{e}^i_{l,T_\delta})_\mathcal{W}$, we therefore define the residual of the a posteriori error estimator as

$$\Delta^i_{l,T_\delta} := \frac{\|\bar{e}^i_{l,T_\delta}\|_\mathcal{W}}{\sqrt{\lambda_{LB}}}. \tag{2.22}$$

Here λ_{LB} is an approximation of the coercivity constant λ defined in (2.2). For the detail of the procedure, we refer to [10, 13]. In the context of the RB-FE-HMM [9], the output of interest is the effective tensor at a given $x_\tau \in \Omega$. The error of this quantity can be shown to be bounded by $(\Delta^i_{l,T_\delta})^2$, i.e.,

$$|(a^0_{\mathcal{N},T_\delta}(x_\tau))_{ii} - (a^0_{l,T_\delta}(x_\tau))_{ii}| \leq (\Delta^i_{l,T_\delta})^2, \tag{2.23}$$

where $a^0_{\mathcal{N},T_\delta}$ is the numerical homogenized tensor constructed by solving accurately the cell problems (2.16) and a^0_{l,T_δ} is the numerical homogenized tensor (3.36) obtained from the RB solutions of the cell problem (2.16).

We summarize the algorithm for the offline procedure.

Algorithm 2.1. *Denote by $\|\cdot\|_{\mathcal{W}}$ the norm associated to the space $W(Y)$ (defined by (2.5) or (2.4)). Given two parameters, N_{RB} the maximum basis number, and tol_{RB} a stopping tolerance.*

1. *Choose randomly N_{train} sampling domains T_{δ_n} (N_{train} large enough and $T_{\delta_n} \subset \Omega$). Define the "training set" $\Xi_{RB} = \{(T_{\delta_n}, \eta_n); 1 \leq \eta_n \leq d, 1 \leq n \leq N_{train}\}$.*

2. *Compute $\hat{\xi}^{\eta_1}_{\mathcal{N},T_{\delta_1}}$, corresponding to $(T_{\delta_1}, \eta_1) \in \Xi_{RB}$. Let $\hat{\xi}_{1,\mathcal{N}}(y) = \frac{\hat{\xi}^{\eta_1}_{\mathcal{N},T_{\delta_1}}(y)}{\|\hat{\xi}^{\eta_1}_{\mathcal{N},T_{\delta_1}}\|_{\mathcal{W}}}$, and the corresponding RB space $S_1(Y) = span\{\hat{\xi}_{1,\mathcal{N}}\}$.*

3. *For $l = 2, \ldots, N_{RB}$*

   a. *select $(T_{\delta_l}, \eta_l) = argmax_{(T_\delta,\eta)\in\Xi_{RB}} \Delta^{\eta}_{l-1,T_\delta}$, provided that $\max_{(T_\delta,\eta)\in\Xi_{RB}} (\Delta^{\eta}_{l-1,T_\delta})^2 > tol_{RB}$, otherwise the algorithm ends;*

   b. *compute $\hat{\xi}^{\eta_l}_{\mathcal{N},T_{\delta_l}}$ corresponding to the selected parameters (T_{δ_l}, η_l). Set $\hat{\xi}_{l,\mathcal{N}}(y) = \frac{R_l(y)}{\|R_l(y)\|_{\mathcal{W}}}$ the $l-th$ RB basis function, where*

$$R_l(y) = \hat{\xi}^{\eta_l}_{\mathcal{N},T_{\delta_l}}(y) - \sum_{m=1}^{l-1} (\hat{\xi}^{\eta_l}_{\mathcal{N},T_{\delta_l}}, \hat{\xi}_{m,\mathcal{N}}) \hat{\xi}_{m,\mathcal{N}}.$$

   Define the RB space $S_l(Y) = span\{\hat{\xi}_{1,\mathcal{N}}, \ldots, \hat{\xi}_{l,\mathcal{N}}\}$.

4. *End For.*

We emphasize that thanks to the affine representation of the tensor, the computation of the a posteriori error estimator (2.22) does not involve the solution of large linear systems for each iteration. Instead, only a linear combination of a few parameter independent FE solutions needs to be computed for each element of the training set Ξ_{RB}, see [11, 12].

Output of the offline procedure. The output of the above procedure is the RB space

$$S_N(Y) = \text{span}\{\hat{\xi}_{n,\mathcal{N}}(y),\ n = 1, .., N\}. \tag{2.24}$$

Rather than storing the reduced basis, using the affine representation (2.18) described above, the output consists of the following matrices and vectors

$$(A_q)_{nm} := \int_Y a_q(y) \nabla \hat{\xi}_{n,\mathcal{N}}(y) \cdot \nabla \hat{\xi}_{m,\mathcal{N}} dy, \quad (F^i_q)_m := \int_Y a_q(y) \mathbf{e_i} \cdot \nabla \hat{\xi}_{m,\mathcal{N}}(y) dy. \tag{2.25}$$

Online procedure of the RB-FE-HMM. We define a macro method similar to the FE-HMM, with micro functions computed in the RB space. The method reads: find $u^{H,RB} \in S^{\ell}_0(\Omega, \mathcal{T}_H)$ such that

$$B_{H,RB}(u^{H,RB}, v^H) = \int_\Omega f v^H dx,\ \forall v^H \in S^{\ell}_0(\Omega, \mathcal{T}_H), \tag{2.26}$$

with a bilinear form given by

$$B_{H,RB}(v^H, w^H) := \sum_{K\in\mathcal{T}_H}\sum_{j=1}^{J}\frac{\omega_{K_j}}{|K_{\delta_j}|}\int_{K_{\delta_j}} a^\varepsilon(x)\nabla v_{N,K_j}(x)\cdot\nabla w_{N,K_j}(x)dx, \tag{2.27}$$

where $v_{N,K_j}(x)$ (respectively $w_{N,K_j}(x)$) is such that $v_{N,K_j} - v^H_{lin,j}(x) \in S_N(K_{\delta_j})$ and

$$\int_{K_{\delta_j}} a^\varepsilon(x)\nabla v_{N,K_j}(x)\cdot\nabla z_N(x)dx = 0, \quad \forall z_N \in S_N(K_{\delta_j}). \tag{2.28}$$

The space $S_N(K_{\delta_j})$ is defined through the mapping $G_{x_{K_j}} : Y \to K_{\delta_j}$ as

$$S_N(K_{\delta_j}) = \text{span}\{\delta\hat{\xi}_{n,\mathcal{N}}(G^{-1}_{x_{K_j}}(x)) =: \xi_{n,K_j}(x),\ n = 1,..,N\}. \tag{2.29}$$

Owing to the affine form (2.18) of the tensor a^ε, the problem (2.28) amounts to solve an $N\times N$ linear system (recall N is small). Indeed, we observe that by writing $v_{N,K_j} - v^H_{lin,j}(x) = \sum_{n=1}^N \alpha_n\xi_{n,K_j}(x)$ (2.28) reads

$$\sum_{n=1}^{N}\alpha_n\int_{K_{\delta_j}} a^\varepsilon(x)\nabla\xi_{n,K_j}(x)\cdot\nabla\xi_{m,K_j}(x)dx = -\sum_{i=1}^{d}\int_{K_{\delta_j}} a^\varepsilon(x)\mathbf{e_i}\cdot\nabla\xi_{m,K_j}(x)dx\frac{\partial v^H_{lin,j}}{\partial x_i}, \tag{2.30}$$

for all $m = 1,\dots N$. Next, thanks to the affine representation of the tensor (see (2.18)), (2.30) can be written as

$$\left(\sum_{q=1}^{Q}\Theta_q(x_{K_j})A_q\right)\boldsymbol{\alpha} = -\sum_{i=1}^{d}\left(\sum_{q=1}^{Q}\Theta_q(x_{K_j})F^i_q\right)\frac{\partial v^H_{lin,j}}{\partial x_i}, \tag{2.31}$$

where the $N\times N$ matrices $A_q,\ q = 1,\dots,Q$ and the vectors $F^i_q \in \mathbb{R}^N,\ q = 1,\dots,Q,\ i = 1,\dots,d$ are defined by (2.25).

Remark 2.2. *It is proved in [9] that problem* (2.26) *has unqiue solution.*

A priori error analysis. We recall the results obtained in [9] that will be useful in the sequel. Assume that $u^0 \in H^{\ell+1}(\Omega)$, that (**Q1**), (**Q2**) and (2.2) hold and that the homogenized tensor $a^0(x)$ is sufficiently regular, then we have

$$\|u^0 - u^{H,RB}\|_{H^1(\Omega)} \le C(H^\ell + r_{HMM}), \quad \|u^0 - u^{H,RB}\|_{L^2(\Omega)} \le C(H^{\ell+1} + r_{HMM}),$$

where

$$r_{HMM} = \sup_{K\in\mathcal{T}_H}\sup_{x_{K_j}\in K}\|a^0(x_{K_j}) - a^0_N(x_{K_j})\|_{\mathcal{F}}, \tag{2.32}$$

and where $a^0_N(x_{K_j})$ is defined in (3.36) and $a^0(x_{K_j})$ is the tensor of the homogenized problem (2.3) evaluated at the quadrature point x_{K_j}.

It can be seen in the above convergence rates, that the error in the macro FE space is optimal in the L^2 or H^1 norm. The term r_{HMM} can be further decomposed as $r_{HMM} = r_{MOD} + r_{MIC} + r_{RB}$, where r_{MOD} stands for the HMM modelling error, r_{MIC} stands for the micro error and r_{RB} stands for the reduced basis error. The error bounds for r_{MOD} and r_{MIC} can be obtained following the analysis for (2.12) (2.13) and (2.10) presented in [7, 8, 26, 9]. In the RB-FE-HMM, r_{MIC} is introduced by using numerical methods to compute the RB functions. Since we require the RB functions to be accurately computed, r_{MIC} is small. The last error term r_{RB} arises from using the RB space $S_N(Y)$ to approximate the infinite dimensional space $\mathcal{M}^{\mathcal{N}}(Y)$ defined in (2.17). Under appropriate smoothness assumption on the macro variation of the tensor $a^\varepsilon(x)$, one can expect fast decay of r_{RB} (e.g., exponential decay [32, 33]). For completeness, we recall the a priori error analysis derived in [9].

Theorem 2.3. *In addition to the assumptions stated above, we assume that the parametrized cell solution space $\mathcal{M}^{\mathcal{N}}$ has an exponentially small Komogorov N-width $d_N(\mathcal{M}^{\mathcal{N}}, W) \leq ce^{-rN}$, where r satisfies $r > \log(1 + (\Lambda/\lambda_{LB})\sqrt{\Lambda/\lambda})$. Then,*

$$\|u^0 - u^{H,RB}\|_{H^1(\Omega)} \leq C(H^\ell + e^{-2sN} + \Big(\frac{h}{\varepsilon}\Big)^{2q} + r_{MOD}), \tag{2.33}$$

$$\|u^0 - u^{H,RB}\|_{L^2(\Omega)} \leq C(H^{\ell+1} + e^{-2sN} + \Big(\frac{h}{\varepsilon}\Big)^{2q} + r_{MOD}), \tag{2.34}$$

where Komogorov N-width $d_N(\mathcal{M}^{\mathcal{N}}, W)$ is defined as

$$d_N(\mathcal{M}^{\mathcal{N}}, W) \;=\; \inf\{\sup_{x\in\mathcal{M}^{\mathcal{N}}} \inf_{y\in W_N} \|x-y\|_{\mathcal{W}} : W_N(Y) \text{ a } N-\text{dimensional subspace of } W(Y)\}.$$

Remark 2.4. *The term r_{MOD} in* (2.33) *and* (2.34) *can be estimated by* (2.12) *and* (2.13) *under suitable assumptions, see [9].*

3. The energy norm based adaptive RB-FE-HMM

In this section, we introduce the adaptive RB-FE-HMM. For simplicity, we only consider simplicial macro FEs in what follows (notice that for such elements **(Q2)** implies **(Q1)**, see Section 2.1). We start by discussing a posteriori error estimates in the energy norm. Such results have first been obtained for the FE-HMM in [21]. To obtain a more efficient algorithm, we apply the RB strategy for the adaptive FE-HMM and in turn avoid having to refine the micro mesh simultaneously to the adaptive macro mesh refinement.

Reduced basis multiscale jump and flux. It is shown in [9] that the RB-FE-HMM bilinear form can be reformulated as,

$$B_{H,RB}(v^H, w^H) := \sum_{K\in\mathcal{T}_H} \sum_{j=1}^{J} \omega_{K_j} a_N^0(x_{K_j}) \nabla v_{lin,j}^H(x_{K_j}) \cdot \nabla w_{lin,j}^H(x_{K_j}), \tag{3.35}$$

where

$$(a_N^0(x_{K_j}))_{ik} = \int_Y a_{x_{K_j}}(y) \left(\nabla \hat{\chi}_{N,K_j}^i(y) + \mathbf{e_i}\right) \cdot \left(\nabla \hat{\chi}_{N,K_j}^k(y) + \mathbf{e_k}\right) dy, \tag{3.36}$$

and $\hat{\chi}^i_{N,K_j}(y)$ is the solution of (2.16) in the RB space (2.24). In view of (2.14) and the mapping G_{x_τ}, defined in Section 2.2, $v_{N,K_j}(x)$ the solution of (2.28) can be expressed as

$$v_{N,K_j}(x) = v^H_{lin,j}(x) + \delta \sum_{i=1}^{d} \hat{\chi}^i_{N,K_j}(G^{-1}_{x_{K_j}}(x)) \frac{\partial v^H_{lin,j}}{\partial x_i}. \tag{3.37}$$

Furthermore (3.36) can be written in the following form (see [27]),

$$a^0_N(x_{K_j}) = \int_Y a_{x_{K_j}}(y) \left(I + J^T_{\hat{\chi}^i_{N,K_j}}(y) \right) dy, \tag{3.38}$$

where $J_{\hat{\chi}^i_{N,K_j}}$ is a $d \times d$ tensor, defined as $(J_{\hat{\chi}^i_{N,K_j}}(y))_{ik} = (\partial \hat{\chi}^i_{N,K_j})/(\partial y_k)$. Therefore one can show that for $\forall v^H \in S^\ell_0(\Omega, \mathcal{T}_H)$ the relation below holds (see [28])

$$\frac{1}{|K_{\delta_j}|} \int_{K_{\delta_j}} a_{x_{K_j}}(G^{-1}_{x_{K_j}}(x)) \nabla v_{N,K_j}(x) dx = a^0_N(x_{K_j}) \nabla v^H(x_{K_j}). \tag{3.39}$$

We introduce in each macro element K the interpolation polynomial $\Pi^K_{a\nabla v_N}(x) \in \mathcal{P}^{l-1}(K)$ following [28, 21] which satisfies

$$\Pi^K_{a\nabla v_N}(x_{K_j}) = \frac{1}{|K_{\delta_j}|} \int_{K_{\delta_j}} a_{x_{K_j}}(G^{-1}_{x_{K_j}}(x)) \nabla v_{N,K_j}(x) dx, \ j = 1, \cdots, \mathcal{L}, \tag{3.40}$$

where $\mathcal{L}$ is the number of quadrature points in one element. The polynomial $\Pi^K_{a\nabla v_N}$ is called "multiscale flux". Combing (3.39) with (3.40), we have

$$\Pi^K_{a\nabla v_N}(x_{K_j}) = a^0_N(x_{K_j}) \nabla v^H(x_{K_j}). \tag{3.41}$$

Remark 3.1. *The interpolation polynomial is uniquely determined by condition* (3.40)*, provided* **(Q2)** *holds and*

$$\begin{aligned} \mathcal{L} &= \frac{1}{2}\ell(\ell+1) \quad d = 2, \\ \mathcal{L} &= \frac{1}{6}\ell(\ell+1)(\ell+1) \quad d = 3. \end{aligned} \tag{3.42}$$

With such a choice for $\mathcal{L}$, one can deduce that $\Pi^K_{a\nabla v_N}(x) \in \mathcal{P}^{\ell-1}(K)$ (see [21, 22]).

We denote by K^+ and K^- two macro elements with a non empty interface given by $e = K^+ \cap K^-$. Now we define the RB multiscale jump on the interior interface e as

$$[\![\overline{\Pi^K_{a\nabla v_N}}]\!]_e(s) := \begin{cases} (\Pi^{K^+}_{a\nabla v_N}(s) - \Pi^{K^-}_{a\nabla v_N}(s)) \cdot n_e & \text{for } e \not\subset \partial\Omega, \\ 0 & \text{for } e \subset \partial\Omega, \end{cases} \tag{3.43}$$

where n_e is the outward normal vector of e on ∂K^+.

Remark 3.2. *When the macro FE space is $S_0^1(\Omega,\mathcal{T}_H)$ with simplicial element, $\mathcal{L}=1$ and we have only one quadrature point per macro element. Then* (3.43) *can be simply written as*

$$[\![\overline{a^\varepsilon \nabla v_{N,K}}]\!]_e := \begin{cases} \Big(\frac{1}{|K_\delta^+|}\int_{K_\delta^+} a_{x_{K^+}}(G^{-1}_{x_{K^+}}(x))\nabla v_{N,K^+}(x)dx - \\ \frac{1}{|K_\delta^-|}\int_{K_\delta^-} a_{x_{K^-}}(G^{-1}_{x_{K^-}}(x))\nabla v_{N,K^-}(x)dx\Big)\cdot n_e & \text{for } e\not\subset\partial\Omega, \\ 0 & \text{for } e\subset\partial\Omega. \end{cases} \tag{3.44}$$

The energy norm based a posteriori error estimates. Following [22], we introduce the local refinement indicator and the data approximation error.

Definition 3.3. *The local refinement indicator $\eta_H(K)$ is defined by*

$$\eta_H(K)^2 := H_K^2\|f^H+\nabla\cdot\Pi^K_{a\nabla u_N}(x)\|^2_{L^2(K)} + \frac{1}{2}\sum_{e\subset\partial K} H_e\|[\![\overline{\Pi^K_{a\nabla u_N}}]\!]_e(s)\|^2_{L^2(e)}, \tag{3.45}$$

and the local data approximation error is defined by

$$\xi_H(K)^2 := H_K^2\|f^H-f\|^2_{L^2(K)} + \|\Pi^K_{a\nabla u_N}(x)-a^0(x)\nabla u^{H,RB}\|^2_{L^2(\Omega)}, \tag{3.46}$$

where a^0 is the tensor of the homogenized problem (2.3) *and f^H is an approximation of f in the space $\{g\in L^2(\Omega), g|_K\in\mathcal{P}^m(K),\forall K\in\mathcal{T}_H\}$.*

Remark 3.4. *If the macro FE space is $S_0^1(\Omega,\mathcal{T}_H)$, the local refinement indicator and local data approximation can be written respectively, in the following way,*

$$\eta_H(K)^2 := H_K^2\|f^H\|^2_{L^2(K)} + \frac{1}{2}\sum_{e\subset\partial K} H_e\|[\![\overline{a^\varepsilon\nabla u_{N,K}}]\!]_e(s)\|^2_{L^2(e)}, \tag{3.47}$$

$$\xi_H(K)^2 := H_K^2\|f^H-f\|^2_{L^2(K)} + \|(a^0_N(x)-a^0(x))\nabla u^{H,RB}\|^2_{L^2(\Omega)}. \tag{3.48}$$

We now explain how we obtain the expressions of the local indicator (3.45) and data approximation (3.46).

Lemma 3.5. *Define $e^H=u^0-u^{H,RB}$. For $\forall v\in H_0^1(\Omega)$, the following representation formula holds*

$$\begin{aligned} B_0(e^H,v) &= \int_\Omega f^H v dx - \sum_{K\in\mathcal{T}_H}\Big(\sum_{e\subset\partial K}\int_e [\![\overline{\Pi^K_{a\nabla u_N}}]\!]_e(s)v ds + \int_K \nabla\cdot\Pi^K_{a\nabla u_N}(x)v dx \\ &+ \int_K(\Pi^K_{a\nabla u_N}(x)-a^0(x)\nabla u^{H,RB})\cdot\nabla v dx + \int_K (f-f^H)v dx\Big), \end{aligned} \tag{3.49}$$

where $B_0(\cdot,\cdot)$ is the bilinear form of the homogenized equation (2.3).

Expression (3.49) is instrumental to derive upper and lower a posteriori error bounds.

Proof. The proof follows [21, Lemma 9] and we sketch the idea. First we write

$$B_0(e^H, v) = \int_\Omega f v dx - \sum_{K\in\mathcal{T}_H} \int_K a^0(x)\nabla u^{H,RB}\nabla v dx.$$

We then add and subtract the term $\sum_{K\in\mathcal{T}_H}\int_K \Pi^K_{a\nabla u_N}(x)\cdot\nabla v + f^H v dx$ in the above expression, use integration by part for the expression $\sum_{K\in\mathcal{T}_H}\int_K a^0(x)\nabla u^{H,RB}\nabla v dx$, to finally obtain (3.49). □

The following two theorems give upper and lower bounds of the error $\|u^0 - u^{H,RB}\|_{H^1(\Omega)}$ in terms of the local refinement indicator $\eta_H(K)$ and local data approximation error $\xi_H(K)$. As the proofs of the theorems are very similar to those in [21], we only sketch them here for completeness.

Theorem 3.6. *(A posteriori upper bound) Let* $\eta_H(\Omega)^2 = \sum_{K\in T_H}\eta_H(K)^2$, $\xi_H(\Omega)^2 = \sum_{K\in T_H}\xi_H(K)^2$. *There exists a constant* $C > 0$, *such that*

$$\|u^0 - u^{H,RB}\|^2_{H^1(\Omega)} \le C(\eta_H(\Omega)^2 + \xi^2_H(\Omega)).$$

Sketch of the proof: Due to the low regularity of the exact solution (only assumed to be in $H^1(\Omega)$), one considers the Clément interpolation operator $I^H e^H$ of $e^H = u^0 - u^{H,RB}$, where $I^H e^H \in S^1_0(\Omega, \mathcal{T}_H)$ (see [34]). By adding the equation $B_{H,RB}(u^{H,RB}, I^H e^H) - \sum_{K\in\mathcal{T}_H}\int_K f I^H e^H dx = 0$ to (3.49) and writing $\psi^H = e^H - I^H e^H$, we obtain

$$\begin{aligned} B_0(e^H, e^H) &= \int_\Omega f^H\psi^H dx + \sum_{K\in\mathcal{T}_H}\Big(\int_K \nabla\cdot\Pi^K_{a\nabla u_N}(x)\psi^H dx + \sum_{e\in\partial K}\int_e \overline{[\![\Pi^K_{a\nabla u_N}]\!]}_e(s)\psi^H ds\Big) \\ &+ \int_\Omega (f - f^H)\psi^H dx + \sum_{K\in\mathcal{T}_H}\int_K (\Pi^K_{a\nabla u_N}(x) - a^0(x)\nabla u^{H,RB})\cdot\nabla e^H dx. \end{aligned}$$

The upper bound can then be obtained by using the Cauchy-Schwarz inequality and the property $\|\psi^H\|_{L^2(K)} \le CH\|\nabla e^H\|_{L^2(K)}$ of the Clement interpolation operator to the above expression.

Theorem 3.7. *(A posteriori lower bound) There exists a constant* C *such that*

$$\eta_H(K)^2 \le C(\|u^0 - u^{H,RB}\|^2_{H^1(\omega_K)} + \xi_H(\omega_K)^2),$$

where ω_K *is the union of all the elements sharing an interface with* K.

Sketch of the proof: The first step is to estimate the term $H_K^2\|f^H + \nabla\cdot\Pi^K_{a\nabla u_N}(x)\|^2_{L^2(K)}$ in (3.45) which is the so called interior residual. For that, one needs to consider an interior bubble function ψ_K in an FE space defined over a refinement $\tilde{\mathcal{T}}_H$ of $\mathcal{T}_H$ so that every $K \in \mathcal{T}_H$ has an interior node $\tilde{x}_K$ in $\tilde{\mathcal{T}}_H$ (likewise every edge e of $\tilde{\mathcal{T}}_H$ not on the boundary $\partial\Omega$ mush have an interior node in $\tilde{\mathcal{T}}_H$). For any $K \in \mathcal{T}_H$, ψ_K has the properties that $0 \le \psi_K \le 1$,

$\psi_K(\tilde{x}_K) = 1$ and $\psi_K = 0 \in \Omega \setminus K$. We choose the test function $v = \psi_K(f^H + \nabla \cdot \Pi^K_{a\nabla u_N})$, insert it into (3.49). By applying the Cauchy-Schwardz inequality and the inverse inequality we obtain

$$H^2 \|f^H + \nabla \cdot \Pi^K_{a\nabla u_N}\|^2_{L^2(K)} \leq C(\|\nabla e^H\|^2_{L^2(K)} + \xi_H(K)^2).$$

The second step of the proof is to estimate the jump residual which corresponds to the second term in (3.45). Now we need to introduce the edge bubble function ψ_e. Assume w_e is the common edge shared by two elements K_1 and K_2. We introduce $\psi_e \in S^\ell_0(\Omega, \mathcal{T}_H)$ which satisfies $\psi_e(x_{w_e}) = 1$, $\psi_e|_{\partial w_e} = 0$ and choose the test function $v(x)$ such that

$$v(x) = \begin{cases} \overline{[\![\Pi^K_{a\nabla u_N}]\!]_e(s)}\psi_e & x \in K_1 \cup K_2, \\ 0 & x \in \Omega \setminus (K_1 \cup K_2). \end{cases}$$

Inserting this test function into (3.49) and then using the Cauchy-Schwarz inequlity and the estimate $\|\nabla v\|_{L^2(K)} \leq CH^{-1/2}\|\overline{[\![\Pi^K_{a\nabla u_N}]\!]_e(s)}\psi_e\|_{L^2(w_e)}$, we can show that

$$H\|\overline{[\![\Pi^K_{a\nabla u_N}]\!]_e(s)}\|^2_{L^2(e)} \leq C(\|\nabla e^H\|^2_{L^2(\omega_K)} + \xi_H(\omega_K)^2).$$

Combining the estimates for the interior and the jump residual leads to the claimed lower bound.

Remark 3.8. *Let us have a closer look at the data approximation error. The contribution to the data approximation error given by the term $H^2_K\|f - f^H\|_{L^2(K)}$ depends on the accuracy of the approximation f^H of f. This term also arises in single-scale energy norm adaptive FEM. For the second term $\|\Pi^K_{a\nabla u_N}(x) - a^0(x)\nabla u^{H,RB}\|^2_{L^2(\Omega)}$, if one assumes that $a^\varepsilon(x) = a(x, x/\varepsilon) = a(x, y)$ is Y-periodic in y, $a_{ij}(\cdot, y)|_K$ is constant and $a_{ij}(x, \cdot) \in W^{1,\infty}_{per}(Y)$, for all $i, j = 1, \cdots, d$, one can prove that $\|\Pi^K_{a\nabla u_N}(x) - a^0(x)\nabla u^{H,RB}\|_{L^2(\Omega)} \leq Cr_{HMM}$, where $r_{HMM} = r_{MIC} + r_{RB} + r_{MOD}$ (see Section 4 for details). We note that r_{MIC} and r_{RB} can be estimated similarly as for the RB-FE-HMM. In particular, r_{MIC} will usually be small due to the requirement of having a very accurate FE computation in the offline stage. Likewise r_{RB} will be small (even exponentially decaying with respect to the RB number N) if appropriate smoothness in the macroscopic variation of the macro tensor holds. For locally periodic problems, when the slow variable of the tensor is collocated with quadrature points in the bilinear form* (2.27)*, $r_{MOD} = 0$.*

Algorithm. For the adaptive RB-FE-HMM, one needs to have the offline outputs (see (2.25)) which can be repeatedly used for the online adaptive procedure. The adaptive online strategy is quite similar to the adaptive FE-HMM. The algorithm is however much faster due to the precomputed RB functions. We state here the complete algorithm.

Algorithm 3.9. *The adaptive RB-FE-HMM*

- *Offline stage: Construct the RB space $S_N(Y)$ following Algorithm 2.1 and store the output* (2.25)*.*

- *Online stage:*

1.Solve *Compute the macro solution $u^{H,RB}$ on the current macro mesh by (2.26)-(2.28) and the quantity $\frac{1}{|K_{\delta_j}|}\int_{K_{\delta_j}} a_{x_{K_j}}(G^{-1}_{x_{K_j}}(x))\nabla u_{N,K_j}(x)dx$ at the sampling domains centered at each quadrature point. Store the data for the following step.*

2.Estimate *Construct the RB multiscale flux $\Pi^K_{a\nabla u_N}$ and compute the RB mutliscale jump $[\![\overline{\Pi^K_{a\nabla u_N}}]\!]$. Further, compute the error indicator $\eta_H(K)$ for all $K \in \mathcal{T}_H$. If $\sum_{K\in\mathcal{T}_H}\eta_H(K)^2 < tol$, the process ends otherwise moves to the next step, where tol is given as a stopping criterion.*

3.Mark *Identify the macro elements marked for refinement following a suitable marking strategy, based on the refinement indicator η_H.*

4.Refine *Refine the marked the elements by applying the newest vertex refinement strategy [35] which keeps the conformity of the refined mesh. Go back to Step 1 with the refined macro mesh.*

Several marking strategies have been proposed in the literature, for example, [36, 37, 16]. Here we follow the marking strategy E in [16].

Complexity comparison with the adaptive FE-HMM. Recall that for the adaptive FE-HMM we need to refine the micro mesh simultaneously to the refinement of the macromesh. As a result, the micro problems of the adaptive FE-HMM

- have to be recomputed in each refined macro element;
- have increasing number of DOF at each iteration of the macro refinement procedure.

In contrast with the RB-FE-HMM, the micro problems are solved in the RB space whose dimension is fixed, usually small and computed once for all in the offline stage The efficiency improvement of the adaptive RB-FE-HMM compared with the adaptive FE-HMM is illustrated numerically in Section 5.

4. The Goal Oriented Reduced Basis Adaptive FE-HMM

In this section, we apply the RB technique to another multiscale adaptive method, the DWR FE-HMM [22], which is based on the framework of the dual-weighted residual method. Here we want to know the error in a certain quantity of interest, e.g., the value of the macro solution at a certain point, directional point-wise derivative of the macro solution or the average of the solution on a subdomain etc. Thus, the error estimators are designed to quantify the accuracy in the quantities of interest. In turn, the mesh refinement is constructed in order to improve the accuracy of the computed quantity of interest. Generally, we define a linear bounded functional $J : H^1_0(\Omega) \to \mathbb{R}$ to represent the quantity of interest. The main concern is the macroscopic error $e^H := u^0 - u^{H,RB}$ in the form of quantity of interest, i.e.

$$J(e^H) = J(u^0) - J(u^{H,RB}).$$

The construction of the error estimators relies on a primal problem and a dual problem that are described below. In both primal and dual problems, the use of RB to compute suitable micro problems can significantly improve the efficiency of the DWR FE-HMM.

Primal and dual problems. The primal problem is the homogenized problem (2.3) that reads in weak form

$$B_0(u^0, v) = \int_\Omega f v dx, \ \forall v \in H_0^1(\Omega). \tag{4.50}$$

We use $u^{H,RB}$ to approximate u^0 and consider

$$B_{H,RB}(u^{H,RB}, v^H) = \int_\Omega f v^H dx, \ \forall v^H \in S_0^\ell(\Omega, \mathcal{T}_H). \tag{4.51}$$

The dual problem of (4.50) consists in finding $z^0 \in H_0^1(\Omega)$ which satisfies

$$B_0(\phi, z^0) = J(\phi), \ \forall \phi \in H_0^1(\Omega). \tag{4.52}$$

Thus we can deduce that

$$J(u^0 - u^{H,RB}) = B_0(u^0 - u^{H,RB}, z^0). \tag{4.53}$$

We emphasize that when we say in the sequel that we compute a RB-FE-HMM approximation of (4.50) or (4.52), it should be understood that we compute an effective solution based on the fine scale model for (4.50) or (4.52). Of course we do not assume (4.50) and (4.52) to be available.

We next consider a numerical approximation of (4.52) that will allow to estimate the right-hand side of (4.53). We observe that for u^H (the FE solution without numerical quadrature of the primal problem (4.50)), we have $J(u^0 - u^H) = 0$ if taking an approximation z^H of z^0 from the same FE space as u^H because of the Galerkin orthogonality. It has thus been suggested in [38, 39] to use an FE approximation of the dual problem (4.52) in a higher order polynomial space. The same strategy is used for the RB-FE-HMM. We thus consider the RB-FE-HMM solution $z^{\mathcal{H},\mathcal{RB}}$ of (4.52) in the FE space $S^{\hat{\ell}}(\Omega, \mathcal{T}_H)$, $\hat{\ell} > \ell$, i.e. find $z^{\mathcal{H},\mathcal{RB}}$ s.t.

$$B_{\mathcal{H},\mathcal{RB}}(\phi^{\mathcal{H}}, z^{\mathcal{H},\mathcal{RB}}) = J(\phi^{\mathcal{H}}), \quad \forall \phi^{\mathcal{H}} \in S^{\hat{\ell}}(\Omega, \mathcal{T}_H), \tag{4.54}$$

where $B_{\mathcal{H},\mathcal{RB}}$ is the RB-FE-HMM bilinear form (2.27) with an appropriate quadrature scheme (i.e. satisfying **(Q2)** for the higher order polynomial space).

Remark 4.1. *We emphasize that $z^{\mathcal{H},\mathcal{RB}}$ is computed using the same RB space as $u^{H,RB}$ (for the micro functions). Thus the error r_{HMM} is the same for both $z^{\mathcal{H},\mathcal{RB}}$ and $u^{H,RB}$ and fixed after the offline stage. This also means that the cost to solve the micro problems in the online stage does not increase when using higher order macro FE space, since the DOF of the RB space remain unchanged in the online stage.*

The error indicators. Before we define the error indicators, we need to mention the definition of the interior residual $R_{I,H}$ and jump residual $R_{J,H}$. These quantities are given by,

$$R_{I,H}(x)|_K = f^H + \nabla \cdot (\Pi^K_{a\nabla u_N}(x)),$$
$$R_{J,H}(s)|_e = -\frac{1}{2}[\![\overline{\Pi^K_{a\nabla u_N}}]\!]_e(s),$$

where $\Pi^K_{a\nabla u_N}$ and $[\![\overline{\Pi^K_{a\nabla u_N}}]\!]_e(s)$ are defined in (3.40) and (3.43), respectively, and f^H is defined in Definition 3.3.

Next, we give the definition of the local error indicator $\eta_H(K)$ and data approximation $\xi_H(K)$.

Definition 4.2. *The local error indicator is defined as*

$$\eta_H(K) := \int_K R_{I,H}(x) z^{\mathcal{H},\mathcal{RB}} dx + \int_{\partial K} R_{J,H}(x) z^{\mathcal{H},\mathcal{RB}} ds. \tag{4.55}$$

To guide the mesh refinement, we actually use the unsigned local refinement indicator defined as $\bar{\eta}_H(K) = |\eta_H(K)|$ (see [22]).

Remark 4.3. *The unsigned local refinement indicator $\bar{\eta}_H(K)$ leads to a good mesh refinement but not optimal since it is always positive while the global (signed) error indicator (the summation of the element contribution of* (4.55)*) allows cancellation between elements. This cancellation cannot be expressed by $\bar{\eta}_H(K)$ (we notice that finding the optimal mesh is already an issue for single scale DWR). The mesh refinement based on $\bar{\eta}_H(K)$ does nevertheless lead to good convergence rates. One issue is that the decay of the error can have oscillation (see the numerical experiments in Section 5.3).*

In order to analyse the variational crimes introduced for example by using numerical quadrature and computing $z^{\mathcal{H},\mathcal{RB}}$ in the higher order FE space $S^{\hat{\ell}}(\Omega, \mathcal{T}_H)$ etc, we need to introduce a suitable data approximation error.

Definition 4.4. *The data approximation error $\xi_H(K)$ is given by*

$$\begin{aligned} \xi_H(K) &= \int_K (\Pi^K_{a\nabla u_N}(x) - a^0(x)\nabla u^{H,RB}) \cdot \nabla z^{\mathcal{H},\mathcal{RB}} dx \\ &+ B_{0,K}(u^0 - u^{H,RB}, z^0 - z^{\mathcal{H},\mathcal{RB}}) \\ &- \int_K (f^H - f) z^{\mathcal{H},\mathcal{RB}} dx, \end{aligned} \tag{4.56}$$

where $B_{0,K}$ is the bilinear form B_0 restricted to the element K.

The definition of data approximation error is motivated by the following exact DWR RB-FE-HMM error representation.

Theorem 4.5. *The exact representation of the error $e^H = u^0 - u^{H,RB}$ in the quantity of interest is given by*

$$J(e^H) = \sum_{K\in\mathcal{T}_H} \eta_H(K) + \xi_H(K). \tag{4.57}$$

The proof follows [22, Theorem 4]. We sketch the main steps. Considering (4.52) and taking $v = u^0 - u^{H,RB}$, we can deduce

$$J(u^0 - u^{H,RB}) \;=\; B_0(u^0 - u^{H,RB}, z^{\mathcal{H},\mathcal{RB}}) + B_0(u^0 - u^{H,RB}, z^0 - z^{\mathcal{H},\mathcal{RB}}), \tag{4.58}$$

where u^0 is the solution of (4.50), z^0 is the solution of (4.52), $u^{H,RB}$ is the solution of (4.51), and $z^{\mathcal{H},\mathcal{RB}}$ is the solution of (4.54). The last two terms on the right-hand side of (4.58) are part of the data approximation error. The first term can be further written as

$$B_0(u^0 - u^{H,RB}, z^{\mathcal{H},\mathcal{RB}}) = \int_\Omega f^H z^{\mathcal{H},\mathcal{RB}} dx - \int_\Omega (f^H - f) z^{\mathcal{H},\mathcal{RB}} dx + B_0(u^{H,RB}, z^{\mathcal{H},\mathcal{RB}}). \tag{4.59}$$

By the definition of the multiscale flux and integration by parts, one can deduce that

$$\begin{aligned} B_0(u^{H,RB}, z^{\mathcal{H},\mathcal{RB}}) \;&=\; -\sum_{K\in\mathcal{T}_H} \int_K \nabla\cdot(\Pi^K_{a\nabla u_N}(x)) z^{\mathcal{H},\mathcal{RB}} dx \\ &+\; \frac{1}{2}\sum_{K\in\mathcal{T}_H}\sum_{e\subset\partial K} \int_e [\![\overline{\Pi^K_{a\nabla u_N}}]\!]_e(s) z^{\mathcal{H},\mathcal{RB}} ds \\ &-\; \sum_{K\in\mathcal{T}_H} \int_K (\Pi^K_{a\nabla u_N}(x) - a^0(x)\nabla u^{H,RB})\cdot\nabla z^{\mathcal{H},\mathcal{RB}} dx. \end{aligned} \tag{4.60}$$

Combining (4.58) (4.59) and (4.60) proves the theorem.

The following result follows immediately from Theorem.4.5.

Corollary 4.6. *The posteriori upper bound is given by*

$$J(u^0 - u^{H,RB}) \le \sum_{K\in\mathcal{T}_H} \bar{\eta}_H(K) + |\xi_H(K)|.$$

According to the expression (4.57), whether $\sum_{K\in\mathcal{T}_H}\eta_H(K)$ can provide a good approximation to the exact error in the quantity of interest $J(e^H)$ depends on the quality of the data approximation error. The following theorem gives an upper bound for the data approximation error.

Theorem 4.7. *Assume that the triangulation is regular, that the homogenization tensor $a^0(x)$ is smooth enough and that assumption* **(H1)** *and* (2.11) *hold. Assume the condition (***Q2***) holds with $\sigma = 2\ell - 2$ (for primal solution) and $\sigma = 2\hat{\ell} - 2$ (for dual solution). In addition, assume that* (3.42) *holds for the QF for the primal solution and that the multiscale*

tensor $a_{ij}(\cdot, y)$ is locally constant for each $K \in \mathcal{T}_H$. Then we have for $\xi_H(\Omega) = \sum_{K\in\mathcal{T}_H} \xi_H(K)$ the following upper bound

$$|\xi_H(\Omega)| \;\leq\; C\big(H^{\ell+\hat{\ell}} + C\|f - f^H\|_{L^2(\Omega)} + (\frac{h}{\varepsilon})^{2q} + r_{MOD} + r_{RB}\big). \tag{4.61}$$

Proof. We sketch of the proof for this theorem that follows the steps of the proof of [22, Theorem 6]. For the first term of (4.56), we apply the decomposition,

$$\begin{aligned} &\int_K (\Pi^K_{a\nabla u_N}(x) - a^0(x)\nabla u^{H,RB}) \cdot \nabla z^{\mathcal{H},\mathcal{RB}} dx \qquad (4.62)\\ = \;& \underbrace{\int_K (\Pi^K_{a\nabla u_N}(x) - \Pi^K_{a^0\nabla u^{H,RB}}(x)) \cdot \nabla z^{\mathcal{H},\mathcal{RB}} dx}_{I} + \underbrace{\int_K (\Pi^K_{a^0\nabla u^{H,RB}}(x) - a^0(x)\nabla u^{H,RB}) \cdot \nabla z^{\mathcal{H},\mathcal{RB}} dx}_{II}, \end{aligned}$$

where $\Pi^K_{a^0\nabla u^{H,RB}}(x)$ is the interpolation polynomial of $a^0\nabla u^{H,RB}$ on the element K using the same interpolation points as for $\Pi^K_{a\nabla u_N}$. By [22, Lemma 11], we have

$$|I| \leq C(\frac{h}{\varepsilon})^{2q} + r_{MOD} + r_{RB}. \tag{4.63}$$

Next, II vanishes by our assumption on the multiscale tensor.

The second term of the data approximation error defined in (4.56) can be estimated as follows,

$$\begin{aligned} &\sum_{K\in\mathcal{T}_H} |B_{0,K}(u^0 - u^{H,RB}, z^0 - z^{\mathcal{H},\mathcal{RB}})| \\ &\qquad \leq C(H^\ell + (\frac{h}{\varepsilon})^{2q} + r_{MOD} + r_{RB})(H^{\hat{\ell}} + (\frac{h}{\varepsilon})^{2q} + r_{MOD} + r_{RB}). \end{aligned} \tag{4.64}$$

As noticed in Remark 4.1, the dual problem has the same micro and modeling error $(\frac{h}{\varepsilon})^{2q} + r_{MOD} + r_{RB}$ as the primal problem.

The third terms of the data approximation can be bounded as

$$\sum_{K\in\mathcal{T}_H} |\int_K (f^H - f) z^{\mathcal{H},\mathcal{RB}} dx| \leq C\|f^H - f\|_{L^2(\Omega)}. \tag{4.65}$$

Combining (4.63),(4.64) and (4.65) gives the theorem. □

Remark 4.8. *If the FE space for the primal problem is $S^1_0(\Omega, \mathcal{T}_H)$, the assumption on the multiscale tensor in Theorem 4.7 that $a_{ij}(\cdot, y)|_K$ is constant can be removed. In turn, the term II is no longer zero but can be bounded by CH^1 (see [22]).*

Observe from Theorem 4.7 that if r_{RB} is small (e.g., a fast decaying Kolmogorov N-width holds), then the data approximation error for the DWR RB-FE-HMM is smaller than the corresponding data approximation error for the FE-HMM. Indeed, the bound for the micro

error $r_{MIC} \leq C(\frac{h}{\varepsilon})^{2q} = \mathcal{O}(\mathcal{N}^{-\frac{2q}{d}})$ for the RB-FE-HMM, depends on the fine mesh used in the offline stage that is usually smaller than the micro mesh used for the FE-HMM (where a mesh proportional to the macro-mesh is used for efficiency, see the complexity discussion in Section 2.1).

We next summarize our algorithm.

Algorithm 4.9. *(DWR RB-FE-HMM)*

- *Offline stage: Construct the RB space $S_N(Y)$ following Algorithm 2.1 and store the output* (2.25).
- *Online stage:*

1.Solve *On the current macro mesh, first compute the macro solution $u^{H,RB}$ and $\frac{1}{|K_{\delta_j}|}\int_{K_{\delta_j}} a_{x_{K_j}}(G^{-1}_{x_{K_j}}(x))\nabla u_{N,K_j}(x)dx$ at the sampling domains K_{δ_j} of each quadrature point. Then compute the dual solution $z^{\mathcal{H},\mathcal{RB}} \in S^{\hat{\ell}}(\Omega, \mathcal{T}_H)$ also on the current macro mesh. Store the data for the next step.*

2.Estimate *Construct the RB multiscale flux $\Pi^K_{a\nabla u_N}$ and compute the RB mutliscale jump $[\![\overline{\Pi^K_{a\nabla u_N}}]\!]$. Further compute the error indicator $\eta_H(K)$ for all $K \in \mathcal{T}_H$ as an approximation to $J(e^H)$. If $\sum_{K\in\mathcal{T}_H} |\eta_H(K)| < tol$, the process ends otherwise moves to next step, where tol is given as a stopping criterion.*

3.Mark *Mark the macro elements based on $\bar{\eta}_H(K)$ by a given marking strategy (e.g. maximum marking strategy in [36, 37]).*

4.Refine *Refine the marked the elements e.g., by applying the newest vertex refinement strategy which keeps the conformity of the refined mesh. Go back to Step 1 (solve).*

Remark 4.10. *For the DWR FE-HMM, the introduction of the dual problem in each element and its solution using higher order FEM leads to high computational cost (the number of micro problems increases due to the need of using a higher order QF likewise the DOF increase in order to match the accuracy of the increasingly refined macro FE mesh). With the proposed RB strategy, the computation of the micro problems is decoupled from the macro adaptive procedure. Accurate RB functions for the micro problems are computed once and can be used for the primal and dual FE-HMM problems while macro meshes are refined. This brings huge computational saving as can be seen in the numerical experiments.*

5. Numerical Experiments

In this section, we present numerical experiments for the energy norm based adaptive RB-FE-HMM for a 2-D problem on a crack domain in Section 5.1 and a 3-D problem on an L-shape domain in Section 5.2. We also present numerical experiments for the DWR RB-FE-HMM for two types of quantities of interest in Section 5.3. All the numerical simulations are implemented in Matlab R2010b. The core code for the FE-HMM follows [40]. The refinement

strategy and FEM are partly based on AFEM@[35]. In the whole section, we consider the model problem defined in (2.1), with possibly non-homogeneous boundary conditions,

$$\begin{aligned} -\nabla\cdot(a^\varepsilon(x)\nabla u^\varepsilon(x)) &= f \quad \text{in } \Omega, \\ u^\varepsilon(x) &= g_d \quad \text{on } \partial\Omega, \end{aligned} \tag{5.66}$$

where $\varepsilon = 4\times 10^{-5}$. We choose for Section 5.1 and Section 5.3 tensors $a^\varepsilon = a(x,y)$ Y-periodic with respect to y for which explicit expressions of the homogenized tensors are available in order to be able to accurately quantify the errors. We emphasize that the algorithms proposed in this paper are valid for problems with general tensors.

Numerical evaluation of the errors. Let u^H be the numerical solution and u^{ref} be a reference solution (for the effective problem (2.3)) computed on a fine triangulation $\mathcal{T}_h$. The error $u^{ref}-u^H$ in the H^1 and L^2 norms are estimated by

$$\begin{aligned} e_{L^2} &:= \|u^h\|^{-1}_{L^2(\Omega)}\Big(\sum_{K\in\mathcal{T}_h}\sum_{j=1}^{J}\rho_{K_j}|u^H-u^{ref}|(z_{K_j})\Big)^{-1/2}, \\ e_{H^1} &:= \|u^h\|^{-1}_{H^1(\Omega)}\Big(\sum_{K\in\mathcal{T}_h}\sum_{j=1}^{J}\rho_{K_j}|\nabla u^H-\nabla u^{ref}|(z_{K_j})\Big)^{-1/2}, \end{aligned}$$

where we will use $\|u\|_{H^1(\Omega)} \sim (\sum_{K\in\mathcal{T}_H}\|\nabla u\|^2_{L^2(K)})^{1/2}$. Here $\{z_{K_j},\rho_{K_j}\}$ is the quadrature formula on the fine triangulation $\mathcal{T}_h$ chosen to be exact for the degree of the piecewise polynomials used to compute u^{ref}.

5.1. Energy norm based adaptive RB-FE-HMM applied to crack problem

Let $\Omega\subset\mathbb{R}^2$ be a square domain with a crack (see Fig. 1) and let $f=1$, $g_d=0$. The diagonal entries of the multiscale tensor are

$$\begin{aligned} a(x,\frac{x}{\varepsilon})_{11} &= x_1^2+0.2+(x_2+1.2)(\sin(2\pi\frac{x_1}{\varepsilon})+2), \\ a(x,\frac{x}{\varepsilon})_{22} &= x_2^2+0.05+(x_1x_2+1.5)(\sin(2\pi\frac{x_2}{\varepsilon})+2). \end{aligned} \tag{5.67}$$

The corresponding homogenized tensor is also diagonal and can be computed as (see [23, 24])

$$\begin{aligned} a^0(x)_{11} &= \Big(\int_0^1 \frac{1}{x_1^2+0.2+(x_2+1.2)(\sin(2\pi y_1+2)}dy_1\Big)^{-1}, \\ a^0(x)_{22} &= \Big(\int_0^1 \frac{1}{x_2^2+0.5+(x_1x_2+1.5)(\sin(2\pi y_2+2)}dy_2\Big)^{-1}. \end{aligned} \tag{5.68}$$

Offline stage. We use FEM with piecewise linear basis functions (called P1-FEM) as the offline solver to compute the reduced basis functions and set the offline meshsize to 1600×1600 so that the a priori error bound given in Theorem 2.3 reads $r_{MIC}=\mathcal{O}(10^{-7})$. As discussed in [11], the error for the output of interest for the RB method, i.e., the numerical homogenization tensor (2.23), can be bounded by the a posteriori error estimator $max_{(T_\delta,\eta)\in\Xi_{RB}}\,(\Delta^\eta_{N,T_\delta})^2$.

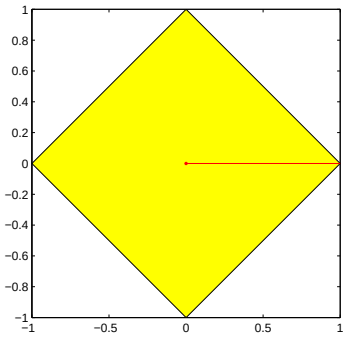

Fig. 1: The domain Ω for the crack problem is in yellow. The red line describes the crack.

In our experiment, this error reads $\mathcal{O}(10^{-11})$ for the particular tolerance chosen (see Table 1) since $max_{(T_\delta,\eta)\in\Xi_{RB}}\ (\Delta^{\eta}_{N,T_\delta})^2 \leq tol_{RB} = \mathcal{O}(10^{-11})$. Furthermore we choose sampling domain sizes of the same length as ε and periodic boundary condition on the cell problems so that $r_{MOD} = 0$ (see (2.12)). As a result of the offline stage, we obtain 10 RB functions (see Table 1 for the parameters related to the offline stage).

Table 1: Parameters for the RB-FE-HMM offline stage.

Solver	P1-FEM
Mesh	1600×1600
Basis number	10
tol_{RB}	5e-11
CPU time(s)	5100

Adaptive P1 RB-FE-HMM online stage. Now we start the adaptive online procedure. Here we present two tests with different online solvers. In the first test we use P1-FEM as the online solver. The corresponding a posteriori error estimator is defined in (3.47). In Fig. 2, we display the macro solution $u^{H,RB}$ after 17 macroscopic iterations of the adaptive RB-FE-HMM.

We recall that the a priori error estimates for RB-FE-HMM derived in Section 2.2 read $\|u^{H,RB} - u^0\|_{H^1(\Omega)} \leq C(H^1 + r_{HMM})$ and $\|u^{H,RB} - u^0\|_{L^2(\Omega)} \leq C(H^2 + r_{HMM})$, where $u^{H,RB} \in S^1_0(\Omega, \mathcal{T}_H)$. We denote by M_{mac} the macro DOF $M_{mac} = \mathcal{O}(H^{-1/2})$ and replace H with $\frac{1}{\sqrt{M_{mac}}}$ in those estimates and obtain

$$\|u^{H,RB} - u^0\|_{H^1(\Omega)} \leq C(\frac{1}{\sqrt{M_{mac}}} + r_{HMM}), \quad \|u^{H,RB} - u^0\|_{L^2(\Omega)} \leq C(\frac{1}{M_{mac}} + r_{HMM}).$$

We see in Fig. 3 that when the macro mesh is refined, the H^1 and L^2 error decay with the optimal rates $\mathcal{O}(M_{mac}^{-1/2})$ and $\mathcal{O}(M_{mac}^{-1})$, respectively. The reference solution u^{ref} is computed with an adaptive FEM with piecewise quadratic polynomials called P2-FEM up

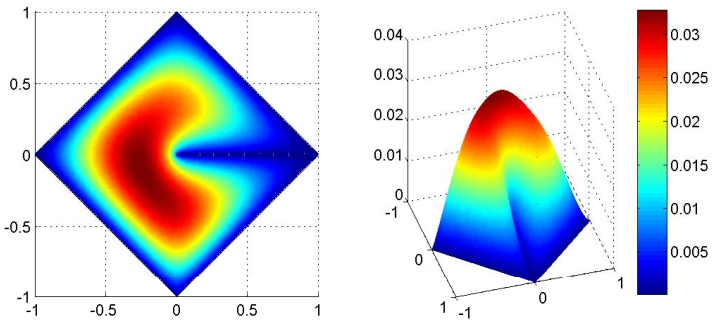

Fig. 2: The adaptive RB-FE-HMM solution computed by P1-FEM on the crack domain.

to 25 iterations with the initial mesh obtained by uniformly refining 2 times the final online mesh (final mesh for $u^{H,RB}$). The number of DOF of u^{ref} is given by 1 757 821. We can also observe in Fig. 3 that the profile of the error indicator is parallel to the H^1 error, which corroborates the estimates of Theorem 3.7.

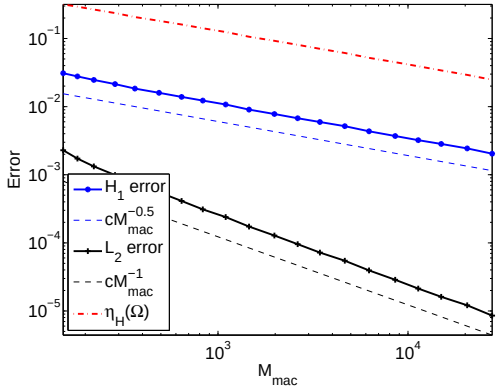

Fig. 3: The refinement indicator $\eta_H(\Omega)$ the H^1 and L^2 errors of the macro solution of the adaptive P1 RB-FE-HMM for 20 iterations.

Adaptive P2 RB-FE-HMM online stage. In this test, we apply the adaptive P2-FEM in the online stage. As we explained in Section 3, an interpolation polynomial $\Pi^K_{a\nabla u_N}$ (see (3.40)) is introduced to define the high order a posteriori error estimator. In this test, $\Pi^K_{a\nabla u_N} \in \mathcal{P}^1(K)$ is interpolated on three quadrature points of the simplicial element. For the P2 RB-FE-HMM, the a priori error estimate yields $\|u^{ref} - u^{H,RB}\|_{H^1(\Omega)}$ proportional to $\mathcal{O}(M_{mac}^{-1})$ and $\|u^{ref} - u^{H,RB}\|_{L^2(\Omega)}$ proportional to $\mathcal{O}(M_{mac}^{-3/2})$. We can observe in Fig. 4 that the errors for the adaptive P2 RB-FE-HMM indeed decay as $\mathcal{O}(M_{mac}^{-1})$ and $\mathcal{O}(M_{mac}^{-3/2})$ in the H^1 and L^2 norms, respectively. We can also observe for the adaptive P2 RB-FE-HMM, that the decay of the error indicator has the optimal H^1 error decay. The reference solution u^{ref} is also computed by an adaptive P2-FEM similarly as described in the first test (but with 20 iterations). The number of DOF is 9 721 276.

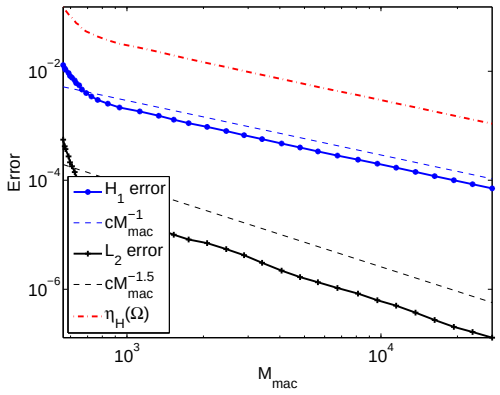

Fig. 4: The refinement indicator $\eta_H(\Omega)$, the H^1 and L^2 errors of the macro solution of the adaptive P2 RB-FE-HMM for 50 iterations.

Comparisons. Here we first compare the efficiency and accuracy of the adaptive RB-FE-HMM with P1-FEM and P2-FEM as macro solvers. We then compare the performance of the adaptive RB-FE-HMM with the adaptive FE-HMM.

- **Adaptive P1 RB-FE-HMM and adaptive P2 RB-FE-HMM.** We first present the online mesh refinements in Fig. 5. The refinements of both P1 and P2 RB-FE-

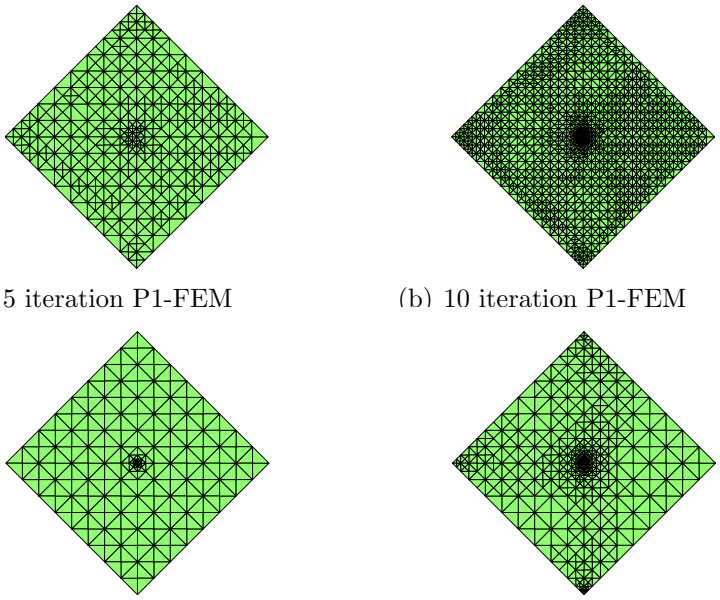

(a) 5 iteration P1-FEM (b) 10 iteration P1-FEM

(c) 10 iteration P2-FEM (d) 20 iteration P2-FEM

Fig. 5: Online refinement. (a) $M_{mac} = 365$. (b) $M_{mac} = 1456$. (c) $M_{mac} = 180$. (d) $M_{mac} = 516$.

HMM can detect the crack and the P2 refinement is more concentrated at the vicinity

of the singularities than the P1 refinement. This higher order macro FEM provides better convergence rates away from the singularities and can therefore use coarser meshes.

Table 2: Comparison of the adaptive P1 RB-HMM-FEM and P2 RB-HMM-FEM.

	P1 RB-FE-HMM	P2 RB-FE-HMM
# iter	20	19
e_{H^1}	0.0020	0.0011
e_{L^2}	8.5412e-06	8.1887e-06
M_{mac}	27725	1750
Total CPU time (s)	25.18	3.92

Now we compare the performance of the two online solvers in Table 2. We can see that for similar errors, the number of the macro DOF M_{mac} for the P2 RB-HMM-FEM is only 6.3% of the M_{mac} for the P1 RB-HMM-FEM and the time cost for the P2 RB-HMM-FEM is 15.6% of the CPU time for the P1 RB-HMM-FEM. This shows the potential advantage of using higher order macro solver for adaptivity.

- **Adaptive P1 RB-FE-HMM and adaptive P1 FE-HMM.** In this numerical experiment, we compare the accuracy and time cost of the adaptive RB-FE-HMM and the adaptive FE-HMM. In Table 3 we presents the total CPU time for 20 iterations, the H^1 error of both methods for each iteration and the corresponding effectivity index which is defined as Eff $:= \frac{\eta_H}{e_{H^1}}$. For this test, the macro error dominates so that in Table 3 the RB-FE-HMM and FE-HMM give almost the same error e_{H^1} and the same effectivity index Eff as the standard adaptive FEM. However, the CPU time comparison immediately shows the advantage of using the adaptive RB-FE-HMM which yields the same accuracy as the adaptive FE-HMM with only 0.14% of its computing time. Even if taking account the offline overhead, the adaptive RB-FE-HMM takes only about 2.8% of the time used for the adaptive FE-HMM.

5.2. The energy norm based adaptive RB-FE-HMM applied to a 3-D problem on an L-shape domain

In this example we investigate the performance of the adaptive RB-FE-HMM on a three dimensional problem. We consider an exponential stationary model for the infiltration of a fluid in unsaturated porous media. We choose here an L-shape computational domain (similar test problems have been considered in [41, 3] for regular domains). The multiscale tensor is defined as

$$a^\varepsilon(x)_{ii} \;=\; 10\alpha^\varepsilon(x)e^{\beta^\varepsilon(x)} + x_1^2 + (x_2 - x_3)^2 + 0.5 \quad i = 1, 2, 3, \tag{5.69}$$

Table 3: Effectivity index and H^1 error for the adaptive RB-FE-HMM, FE-HMM and FEM for the crack problem.

		RB-FE-HMM		FE-HMM		FEM
Iter no.	M_{mac}	e_{H^1}	Eff	e_{H^1}	Eff	Eff
1	153	0.0309	10.2577	0.0309	10.2588	10.2577
2	182	0.0278	10.5756	0.0278	10.5766	10.5756
3	222	0.0247	10.8022	0.0247	10.8031	10.8022
4	287	0.0214	11.0437	0.0214	11.0444	11.0437
5	365	0.0184	11.2158	0.0184	11.2162	11.2158
6	489	0.0159	11.4192	0.0159	11.4196	11.4192
7	643	0.0139	11.5564	0.0139	11.5567	11.5564
8	831	0.0123	11.5224	0.0123	11.5526	11.5224
9	1097	0.0107	11.5932	0.0107	11.5934	11.5932
10	1456	0.0090	11.7484	0.0090	11.7485	11.7484
11	1981	0.0078	11.8570	0.0078	11.8571	11.8570
12	2626	0.0068	11.9613	0.0068	11.9614	11.9613
13	3438	0.0059	11.8667	0.0059	11.8668	11.8667
14	4648	0.0052	11.8540	0.0052	11.8540	11.8540
15	6237	0.0043	11.9844	0.0043	11.9844	11.9844
16	8566	0.0037	12.1085	0.0037	12.1085	12.1085
17	11320	0.0032	12.1627	0.0032	12.1628	12.1627
18	14960	0.0028	11.9973	0.0028	11.9973	11.9973
19	20503	0.0024	11.9997	0.0024	11.9997	11.9997
20	27725	0.0020	12.1779	0.0020	12.1779	12.1779
CPU time for 20 iterations		26.13 s		186110 s		

where

$$\begin{aligned}\beta^\varepsilon(x) &= -\alpha^\varepsilon(x)\big((x_1 - c_1\mu_1(x))^2 + (x_2 - c_1\mu_2(x))^2 + (x_3 - c_1\mu_3(x))^2\big)\cdot \\ &\quad \big((x_1 - 0.8 - c_2\mu_1(x))^2 + (x_2 - 0.5 - c_2\mu_2(x))^2 + (x_3 - 0.7 - c_2\mu_3(x))^2\big), \\ \alpha^\varepsilon(x) &= \frac{1}{10(2 + 1.8\sin(6\pi\frac{x_3}{\varepsilon} - \pi(3\frac{x_1}{\varepsilon} + \frac{x_2}{\varepsilon}))},\end{aligned}$$

and where $\mu(x) = (\mu_1(x), \mu_2(x), \mu_3(x))$ is a uniform random mapping from Ω to $[0,1]^3$ and c_1, c_2 are constant parameters chosen to be $c_1 = 0.2,\ c_2 = 0.1$. We set $f = 10$ and $g_d = 0.5$. In general infiltration models, a^ε represents the microscopic permeability of the porous media. As shown in Fig. 6 (a), we can observe that the media has lowest permeability around points $(0,0,0)$ and $(0.8, 0.5, 0.7)$. When we fix the macro variable to be x^* and map $a^\varepsilon(x)$ to the reference sampling domain $Y = [0,1]^3$ by the mapping G_{x^*} defined in Section 2.2, we obtain the parametrized tensor $a_{x^*}(y)$ with respect to parameter x^* which displays locally periodic pattern shown in Fig. 6 (b). Since the tensor $a^\varepsilon(x)$ in (5.69) is not in an affine form, we need to apply the empirical interpolation method (see [9]) to obtain the affine approximation of

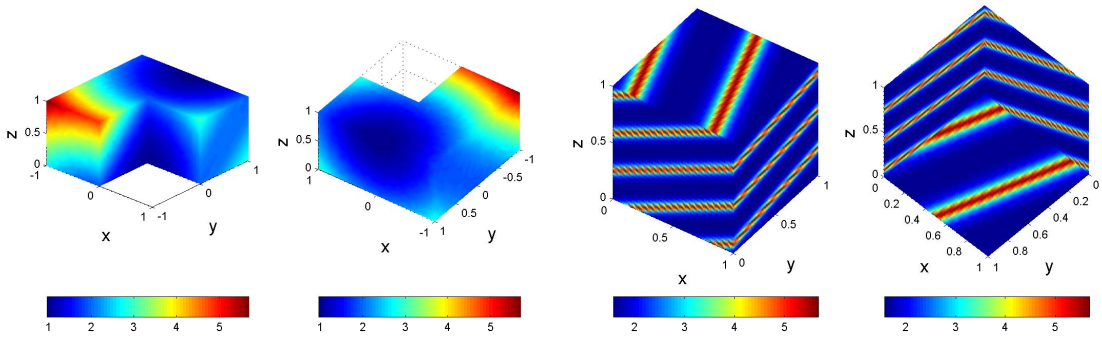

(a) Permeability $a^\varepsilon(x)$ on Ω (b) $a_{x^*}(y)$ on the reference sampling domain

Fig. 6: (a) Permeability $a^\varepsilon(x)$ on the L-shape domain Ω. (b) $a_{x^*}(y)$ on the reference sample domain $Y = [0,1]^3$ with fixed macro variable $x^* = (0.750, 0.625, 0.125)$ and $\mu(x^*) = (0.799, 0.499, 0.643)$.

Table 4: Parameters for the RB-FE-HMM offline stage.

Reference sampling domain Y	$[0,1]^3$
Mesh	200^3
tol_{EIM}	1e-5
tol_{RB}	3e-7
affine terms	11
Basis number	21

the tensor in the offline stage. The offline parameters and output information are presented in Table 4. After the offline stage 21 basis functions are obtained. Constrained by the computation environment, the finest offline mesh generated is 200^3. Considering the macro meshes we test in the online stage (the macroscopic DOF M_{mac} varies in the range of 325 to $63749 \approx 40^3$), the offline mesh is sufficiently fine according to the estimates of Theorem 2.3.

In the online stage, we set the initial macro mesh to be uniform tetrahedron with $M_{mac} = 325$. We perform 24 iterations of the adaptive RB-FE-HMM. The solution $u^{H,RB}$ of the 20th iteration and corresponding macro meshes on the surface of the segment obtained by a cut through the plan $z = 0.5$ are displayed in Fig. 7. As shown in Fig. 8, the mesh refinement mostly takes place in the vicinity of the singularities (the corners of the domain) which also illustrates that the refinement indicators provide effective information for the macro mesh refinement. The error indicator $\eta_H(\Omega)$ for 24 iterations of the adaptive RB-FE-HMM is shown in Fig.9. We observe that the error indicator decays with an optimal convergence rate $\mathcal{O}(M_{mac}^{-1/3})$. This again corroborates the estimates of Theorem 3.6 and Theorem 3.7.

Let us compare the cost to obtain the last iteration with both the RB-FE-HMM and the FE-HMM. The total online CPU time of the RB-FE-HMM for 24 iterations is around 241s. Now we apply the adaptive FE-HMM to this example. The initial macro mesh for the last iteration of the adaptive RB-FE-HMM which

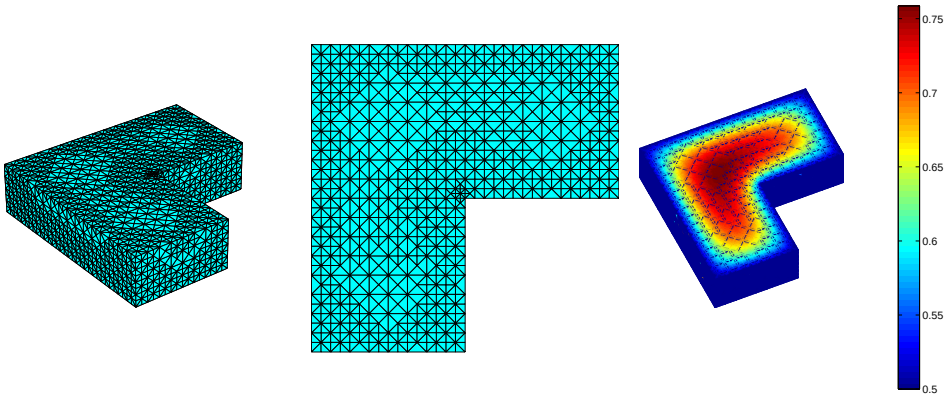

Fig. 7: The macro mesh and $u^{H,RB}$ after 20 iterations.

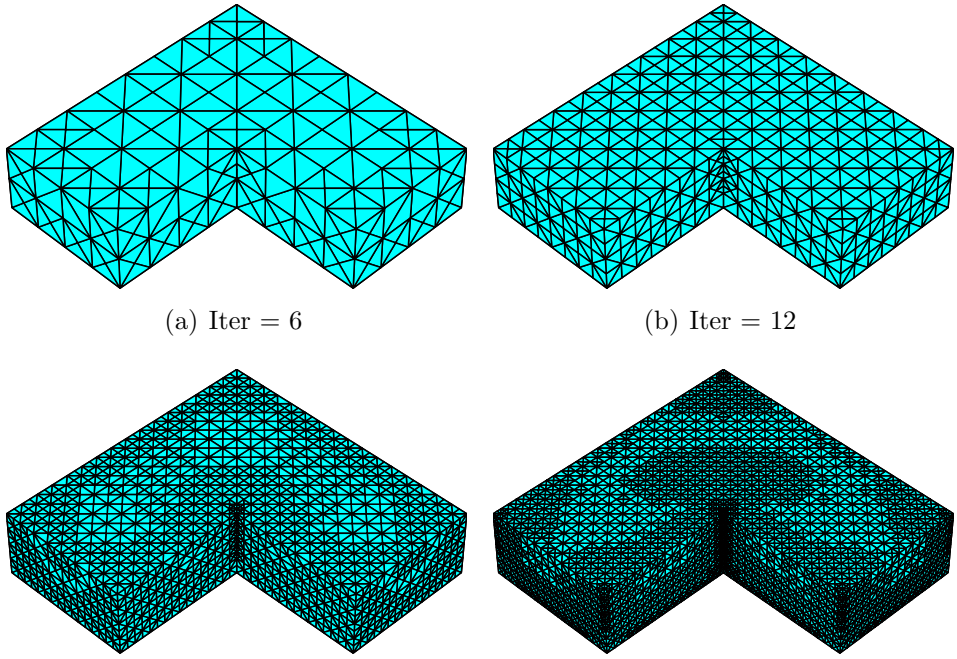

(a) Iter = 6 (b) Iter = 12

(c) Iter = 18 (d) Iter = 24

Fig. 8: The macro mesh refinements.

has 237808 tetrahedra ($M_{mac} \approx 37^3$). The CPU time to compute one cell problem with the average micro meshsize $M_{mic} = 6^3$ and $M_{mic} = 37^3$ is 0.045s and 11s (to obtain the optimal convergence rate in H^1 norm and L^2 norm respectively, one needs to set $M_{mic} = \sqrt{M_{mac}}$ for H^1 norm and $M_{mic} = M_{mac}$ for L^2 norm). Therefore the total CUP time to compute the last

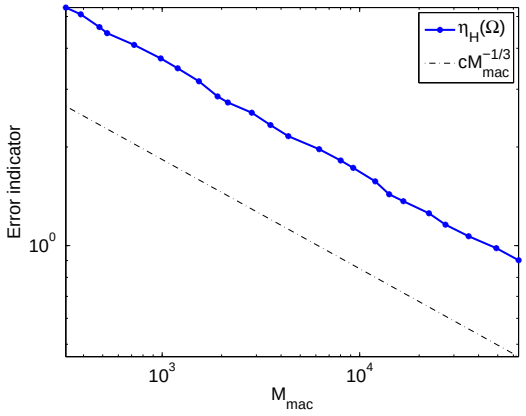

Fig. 9: The a posteriori error decay for adaptivity on the 3-D L-shape domain for 24 iterations.

iteration is about 10701s for H^1 norm refinement and 2615888s for L_2 norm refinement. The advantage of applying the adaptive RB-FE-HMM method to high dimensional problems can thus be seen to be significant.

5.3. DWR RB-FE-HMM.

In this subsection, we present numerical experiment for goal oriented adaptive computations with the DWR RB-FE-HMM. We consider the model equation (5.66) with $f = 1000$, a domain $\Omega = [0, 1]^2$ and the diagonal multiscale tensor given by

$$\begin{aligned} a(x, \frac{x}{\varepsilon})_{11} &= (x_1^2 + 0.2)E + (x_2 + 1.2)(\sin(2\pi\frac{x_1}{\varepsilon}) + 2), \\ a(x, \frac{x}{\varepsilon})_{22} &= (x_2^2 + 0.05)E + (x_1x_2 + 1.5)(\sin(2\pi\frac{x_2}{\varepsilon}) + 2), \end{aligned} \tag{5.70}$$

where

$$E = 1 + 20e^{-1000((x_1-0.5)^2+(x_2-0.5)^2)}.$$

The corresponding homogenized tensor is

$$\begin{aligned} a^0(x)_{11} &= (\int_0^1 \frac{1}{(x_1^2 + 0.2)E + (x_2 + 1.2)(\sin(2\pi y_1 + 2)} dy_1)^{-1}, \\ a^0(x)_{22} &= (\int_0^1 \frac{1}{(x_2^2 + 0.5)E + (x_1x_2 + 1.5)(\sin(2\pi y_2 + 2)} dy_2)^{-1}, \end{aligned} \tag{5.71}$$

which is shown in Fig. 10.

The offline parameters for this example are presented in Table 5. For the online stage, we propose two different types of quantities of interest respectively.

Quantity of interest 1. We use a local average of the macro solution as the quantity of interest defined as

$$J(u^0) = \frac{1}{|\Omega_s|}\int_{\Omega_s} u^0 dx, \tag{5.72}$$

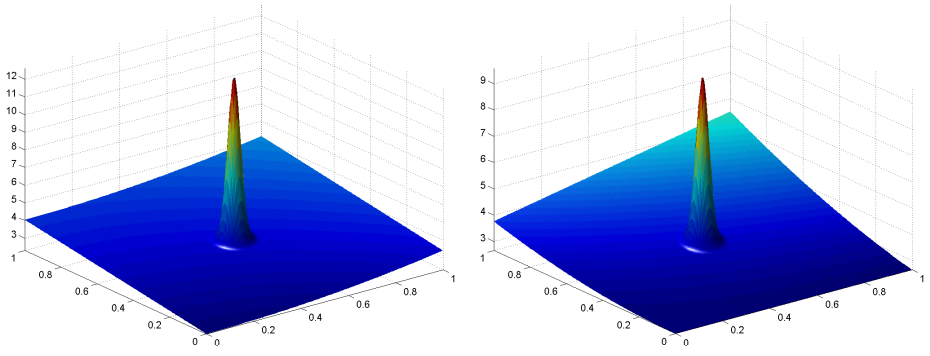

(a) $a^0(x)_{11}$ (b) $a^0(x)_{22}$

Fig. 10: The homogenized tensor (5.71).

Table 5: Parameters for the DWR RB-FE-HMM offline stage

Solver	P1-FEM
Mesh	1600×1600
Basis number	10
tol_{RB}	5e-11
CPU time(s)	6772

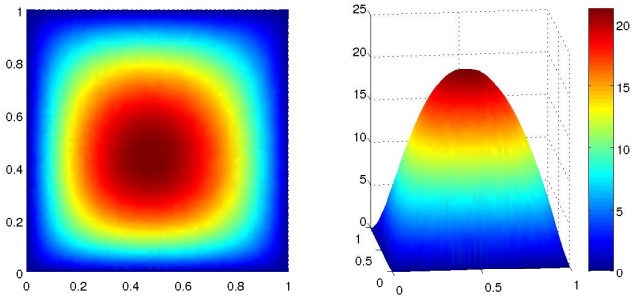

Fig. 11: $u^{H,RB}$ after 11 iterations.

where $\Omega_s \subset \Omega$ is the domain of interest. We choose $\Omega_s = [0.25, 0.5]^2$ in this test. We show in Fig. 11 the solution $u^{H,RB}$ after 10 iterations with 3279 DOF. In Fig.12 (a), we observe that the Eff $:= \frac{|\eta_H(\Omega)|}{J(u^{H,RB}-u^{ref})} \approx 1$ where $\eta_H(\Omega) = \sum_K \eta_H(K)$, which illustrates that the refinement indicator can accurately estimate the error in the quantity of interest and that the data approximation error ξ_H is much smaller than the refinement indicator. In Fig. 12 (b) we observe that the error in quantity of interest converges with a rate of $\mathcal{O}(M_{mac}^{-1})$.

Now we compare the performance of the DWR RB-FE-HMM and DWR FE-HMM. The comparison starts with an initial non-uniform mesh with 289 DOF. For the FE-HMM, we apply the optimal H^1 refinement to the micro problems that is, $h_K = \sqrt{H_K}$ for the P1 micro FEM as the solver for primal problem (4.51) and $h_K = H_K^{2/3}$ for the P2 micro FEM for the

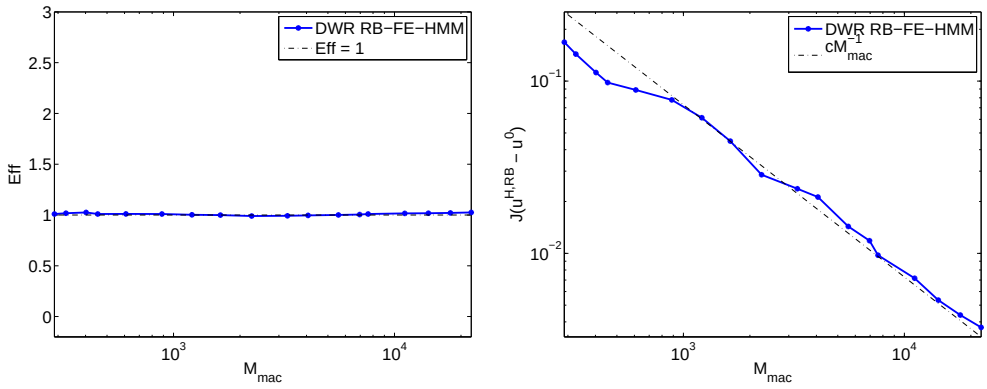

(a) Effectivity index (b) Error in quantity of interest

Fig. 12: The effectivity index and error of the DWR RB-FE-HMM for the quantity of interest (5.72)

dual problem (4.54). According to Fig. 12 (a), $|\eta_H(\Omega)|$ gives a good estimate of the error in the quantity of interest. We can observe in Table. 6 that the two methods yield similar refinements and accuracy while the total online time cost for the DWR RB-FE-HMM is only 0.06% of the time for the DWR FE-HMM (taking into account the offline overhead, the DWR RB-FE-HMM costs only 29% of the computational time for the DWR FE-HMM).

Table 6: The CPU time and refinement indicators of the DWR RB-FE-HMM and the DWR FE-HMM.

	DWR RB-FE-HMM		DWR FE-HMM	
Iter no.	M_{mac}	$\|\eta_H(\Omega)\|$	M_{mac}	$\|\eta_H(\Omega)\|$
1	289	0.1698	289	0.1698
2	326	0.1460	326	0.1460
3	402	0.1150	402	0.1150
4	454	0.0991	454	0.0991
5	609	0.0898	609	0.0898
6	886	0.0785	887	0.0786
7	1212	0.0614	1213	0.0615
8	1630	0.0448	1629	0.0448
CPU time for 8 iterations	14.2		23272	

Quantity of interest 2. In this test we consider a quantity of interest given by

$$J(u^0) = \nabla u^0(x^*) \cdot \bar{s}, \tag{5.73}$$

which represents the pointwise directional derivative (in the direction of the unit vector $\bar{s}$) at $x^* \in \Omega$. We choose $x^* = (0.75, 0.75)$ and $\bar{s} = (\sqrt{2}/2, \sqrt{2}/2)$. Due to the singularity of the right-hand side of the dual problem, one has to approximate this quantity of interest (see [38]). We observe in Fig.13 (a) that the effectivity index varies between 0.15 and 5.8 and when $M_{mac} > 1200$ the effectivity index only varies in a small range from 1 to 1.7 which is close

to the optimal value 1. In Fig. 13 (b), we sketch the rate of the error $J(u^{H,RB} - u^0)$ which approximately decays with an order $\mathcal{O}(M_{mac}^{-1})$ but with large oscillations when $M_{mac} \leq 1200$. The factor which causes the initial oscillations in Fig. 13 might be the strong cancellation effect of the local error indicator $\eta_H(K)$ for coarse macro meshes.

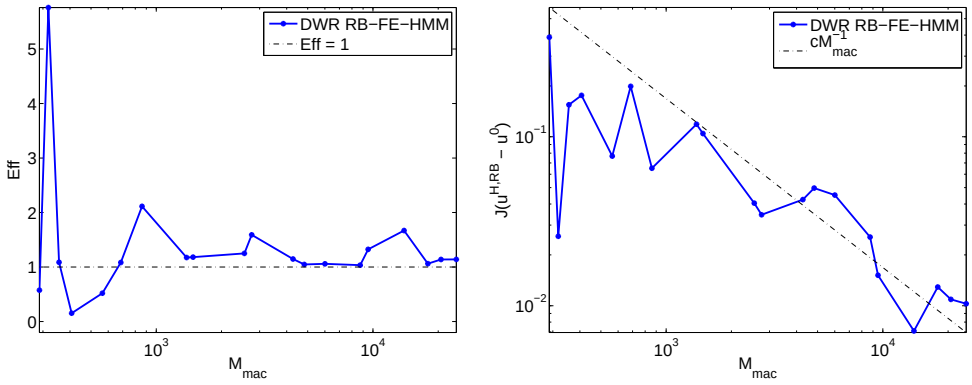

(a) Effectivity index (b) Quantity of interest

Fig. 13: The effectivity index and the error in the quantity of interest for the DWR RB-FE-HMM for 20 iterations (quantity of interest of type 2).

In Fig. 14, we plot the mesh refinement for the two different quantities of interest. We use an initial non-uniform mesh for the tests of the two quantities of interest with meshsize 17×17. After several iterations, the two online meshes show different patterns according to the specific quantity of interest. We can see that in Fig. 14 (a), that the mesh is mostly refined in the target domain Ω_s where the quantity of interest is defined while in Fig. 14 (b), the mesh is more refined around the target point $(0.75, 0.75)$ along the direction $(\sqrt{2}/2, \sqrt{2}/2)$ where the directional derivative is defined. For both quantities of interest, the macro mesh refinements also take place in the vicinity of the singularity where the homogenized tensor has a big jump (i.e., in the center of the domain Ω see Fig. 10).

6. Conclusion

We have presented an efficient adaptive FEM, the RB-FE-HMM, for elliptic homogenization problems based on micro-macro solvers combined with a RB strategy. We have shown that repeated FEM computations of micro problems are avoided during the macro mesh refinement, in contrast to the adaptive FE-HMM, as the micro solutions are computed in a finite dimensional space spanned by a small number of accurately computed representative micro solutions (the reduced basis) obtained by a greedy algorithm in an offline stage. This methodology allows to bypass the derivation of micro a posterior error estimates to calibrate the micro mesh during the macro mesh adaptive cycles. We have presented an a posteriori error analysis for a residual based adaptive RB-FE-HMM. Error estimation for the RB-FE-HMM in quantities of interest has also been presented. The efficiency and the

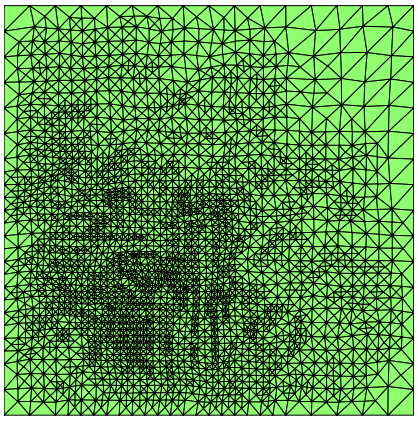

(a) Mesh refinement of quantity of interest 1 (5.72) after 10 iterations, $M_{mac} = 3279$

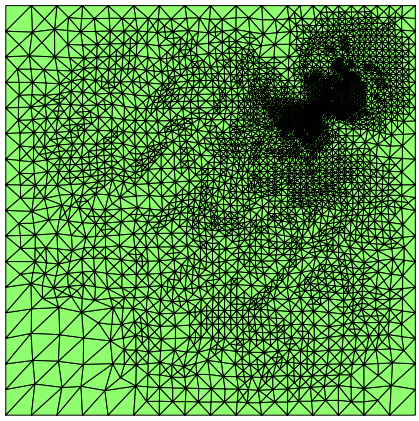

(b) Mesh refinement of quantity of interest 2 (5.73) after 12 iterations, $M_{mac} = 4274$

Fig. 14: The macro meshes for the two quantities of interest.

sharpness of the derived error bounds have been illustrated by several numerical examples in two and three dimensions. These examples show the significant advantage of the adaptive RB-FE-HMM over the adaptive FE-HMM.

Acknowledgements. This work was supported in part by the Swiss National Science Foundation under Grant 200021 134716/1.

References

[1] J. Oden, S. Prudhomme, A. Romkes, P. Bauman, Multiscale modeling of physical phenomena: adaptive control of models, SIAM J. Sci. Comput. 28 (6) (2006) 2359–2389.

[2] A. Abdulle, Analysis of a heterogeneous multiscale FEM for problems in elasticity, Math. Models Methods Appl. Sci. 16 (4) (2006) 615–635.

[3] Y. Efendiev, T. Y. Hou, Multiscale finite element methods. Theory and applications, Vol. 4 of Surveys and Tutorials in the Applied Mathematical Sciences, Springer, New York, 2009.

[4] M. Geers, V. Kouznetsova, W. Brekelmans, Multi-scale computational homogenization: Trends and challenges, J. Comput. Appl. Math. 234 (2010) 2175–2182.

[5] A. Abdulle, W. E, B. Engquist, E. Vanden-Eijnden, The heterogeneous multiscale method, Acta Numer. 21 (2012) 1–87.

[6] W. E, B. Engquist, The heterogeneous multiscale methods, Commun. Math. Sci. 1 (1) (2003) 87–132.

[7] A. Abdulle, The finite element heterogeneous multiscale method: a computational strategy for multiscale pdes, GAKUTO Int. Ser. Math. Sci. Appl. 31 (2009) 135–184.

[8] A. Abdulle, On a priori error analysis of fully discrete heterogeneous multiscale FEM, SIAM, Multiscale Model. Simul. 4 (2) (2005) 447–459.

[9] A. Abdulle, Y. Bai, Reduced basis finite element heterogeneous multiscale method for high-order discretizations of elliptic homogenization problems, J. Comput. Phys., in press.

[10] C. Prud'homme, D. V. Rovas, K. Veroy, L. Machiels, Y. Maday, A. T. Patera, G. Turinici, Reliable real-time solution of parametrized partial differential equations: Reduced-basis output bounds methods, J. Fluids Eng. 124 (2002) 70–80.

[11] A. T. Patera, G. Rozza, Reduced Basis Approximation and A Posteriori Error Estimation for Parametrized Partial Differential Equations, to appear in (tentative rubric) MIT Pappalardo Graduate Monographs in Mechanical Engineering, 2007.

[12] G. Rozza, D. Huynh, A. T. Patera, Reduced basis approximation and a posteriori error estimation for affinely parametrized elliptic coercive partial differential equations, Arch. Comput. Methods. Eng. 15 (2008) 229–275.

[13] S. Boyaval, Reduced-basis approach for homogenization beyond the periodic setting, Multiscale Model. Simul. 7 (1) (2008) 466–494.

[14] S. Boyaval, Mathematical modeling and simulation for material science, PhD thesis, University Paris Est, 2009.

[15] M. Ainsworth, J. Oden, A posteriori error estimation in finite element analysis, John Wiley & Sons, New york, 2000.

[16] R. Verfürth, A review of a posteriori error estimation and adaptive mesh-refinement techniques, Wiley-Teubner, New-York, 1996.

[17] J. Oden, S. Prudhomme, Goal-oriented error estimation and adaptivity for the finite element method, Computers & Mathematics with Applications 41 (5-6) (2001) 735 – 756.

[18] R. Becker, R. Rannacher, An optimal control approach to a posteriori error estimation in finite element methods, Acta numerica 10 (2001) 1–102.

[19] M. Ohlberger, A posteriori error estimates for the heterogeneous multiscale finite element method for elliptic homogenization problems, Multiscale Model. Simul 4 (1) (2005) 88–114.

[20] G. Nguetseng, A general convergence result for a functional related to the theory of homogenization, SIAM J. Math. Anal. 20 (3) (1989) 608–623.

[21] A. Abdulle, A. Nonnenmacher, Adaptive finite element heterogeneous multiscale method for homogenization problems, Comput. Methods Appl. Mech. Engrg. 200 (37-40) (2011) 2710–2726.

[22] A. Abdulle, A. Nonnenmacher, A posteriori error estimate in quantities of interest for the finite element heterogeneous multiscale method, Preprint submitted for publication.

[23] A. Bensoussan, J.-L. Lions, G. Papanicolaou, Asymptotic analysis for periodic structures, North-Holland Publishing Co., Amsterdam, 1978.

[24] V. Jikov, S. Kozlov, O. Oleinik, Homogenization of differential operators and integral functionals, Springer-Verlag, Berlin, Heidelberg, 1994.

[25] P. Ciarlet, P. Raviart, The combined effect of curved boundaries and numerical integration in isoparametric finite element methods, Math. Foundation of the FEM with Applications to PDE (1972) 409–474.

[26] W. E, P. Ming, P. Zhang, Analysis of the heterogeneous multiscale method for elliptic homogenization problems, J. Amer. Math. Soc. 18 (1) (2005) 121–156.

[27] A. Abdulle, A priori and a posteriori error analysis for numerical homogenization: a unified framework, Ser. Contemp. Appl. Math. CAM 16 (2011) 280–305.

[28] A. Abdulle, Discontinuous galerkin finite element heterogeneous multiscale method for elliptic problems with multiple scales, Math. Comp. 81 (278) (2012) 687–713.

[29] A. Abdulle, C. Schwab, Heterogeneous multiscale fem for diffusion problems on rough surfaces, SIAM, Multiscale Model. Simul. 3 (1) (2005) 195–220.

[30] M. Barrault, Y. Maday, N. Nguyen, A. Patera, An 'empirical interpolation method': Application to efficient reduced-basis discretization of partial differential equations, C. R. Acad. Sci. Paris Ser.I 339 (2004) 667–672.

[31] Y. Maday, N. C. Nguyen, A. T. Patera, G. Pau, A general multipurpose interpolation procedure: the magic points, Commun. Pure Appl. Anal. 8 (1) (2009) 383–404.

[32] P. Binev, A. Cohen, W. Dahmen, R. Devore, G. Petrova, P. Wojtaszczyk, Convergence rates for greedy algorithms in reduced basis methods, preprint.

[33] A. Buffa, Y. Maday, A. T. Patera, C. Prud'homme, G. Turinici, A priori convergence of the greedy algorithm for the parametrized reduced basis, to appear in ESAIM-Math. Model. Numer. Anal.Special Issue in honor of David Gottlieb.

[34] P. Clément, Approximation by finite element functions using local regularization., Rev. Franaise Automat. Informat. Recherche Opérationnelle Sér. RAIRO Analyse Numérique 9 (R2) (1975) 77–84.

[35] L. Chenand, C. Zhang, AFEM@matlab: a matlab package of adaptative finite element methods, technical report, 2006.

[36] S. Prudhomme, J. Oden, On goal-oriented error estimation for elliptic problems: application to the control of pointwise errors, Computer Methods in Applied Mechanics and Engineering 176 (1-4) (1999) 313–331.

[37] A. Schmidt, K. Siebert, Design of adaptative finite element software: The finite element toolbox ALBERTA, Vol. 42 of Lecture Notes in Computational Science and Engineering, Springer-Verlag, Berlin, 2005.

[38] W. Bangerth, R. Ranncher, Adaptive finite element methods for differential equations, Birkhäuser Verlag, Basel, 2003.

[39] R. Nochetto, A. Veeser, M. Verani, A safeguarded dual weighted residual method, IMA journal of Numerical Analysis 29 (1) (2009) 126–140.

[40] A. Abdulle, A. Nonnenmacher, A short and versatile finite element multiscale code for homogenization problem, Comput. Methods Appl. Mech. Engrg 198 (37-40) (2009) 2839–2859.

[41] Z. Chen, W. Deng, H. Ye, Upscaling of a class of nonlinear parabolic equations for the flow transport in heterogeneous porous media, Commun. Math. Sci. 3 (4) (2005) 493–515.